166

University of Nevada

Reno

Travel-Times and Crustal Structure in the Nevada Region from

Earthquakes, Nuclear Explosions, and Mine Blasts

A thesis submitted in partial fulfillment of the

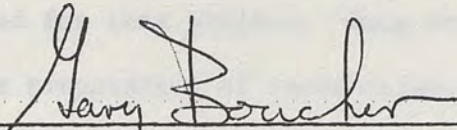requirements for the degree of Master

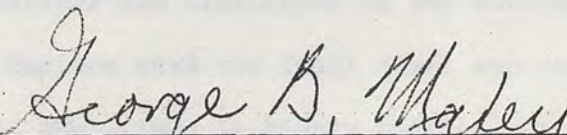of Science in Geophysics
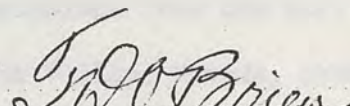

by

Ravi Batra

November 1970

The thesis of Ravi Batra is approved:

_____
Thesis advisor

_____
Department chairman

_____
Dean, Graduate School

University of Nevada

Reno

November 1970

ACKNOWLEDGEMENTS

Table of Contents

List of Figures

List of Figures (Continued)

List of Tables

List of Tables (Continued)

INTRODUCTION

The main purpose of this project was to calibrate a telemetry network of seismographic stations installed in the central part of the State of Nevada (Figure 1). A calibration of this sort is aimed at determining station time delays, if any, and to demonstrate the effectiveness of the network in locating earthquakes, which could then be used for other seismicity studies in the Nevada region. An accurate location of earthquakes (within 2-3 km) requires a detailed knowledge of crustal structure, namely, depths to the Mohorovicic discontinuity at various sites, regional dip, if any, of the crust-mantle interface, presence of an intermediate layer, or layers, within the crust, thicknesses of low-velocity alluvial fills in the region. This project is principally aimed at the determination of the various seismic velocities and crustal structure.

Previous work (see below) on travel times and crustal structure in Nevada, using conventional refraction techniques has covered the eastern and western part of the State, using chemical and nuclear explosions as sources of energy. However, there is an absence of such determinations of velocities and structure in the central part of the State, where most of the earthquakes in the Nevada region are located. Because of the proximity of most of the seismographic stations of the network to the central Nevada seismic zone, knowledge of velocities and crustal structure is required for the accurate determination of epicenters of these events.

This work was initiated at the suggestion of Dr. Alan Ryall, Director, Seismological Laboratory, University of Nevada.

▲ Seismographic station.
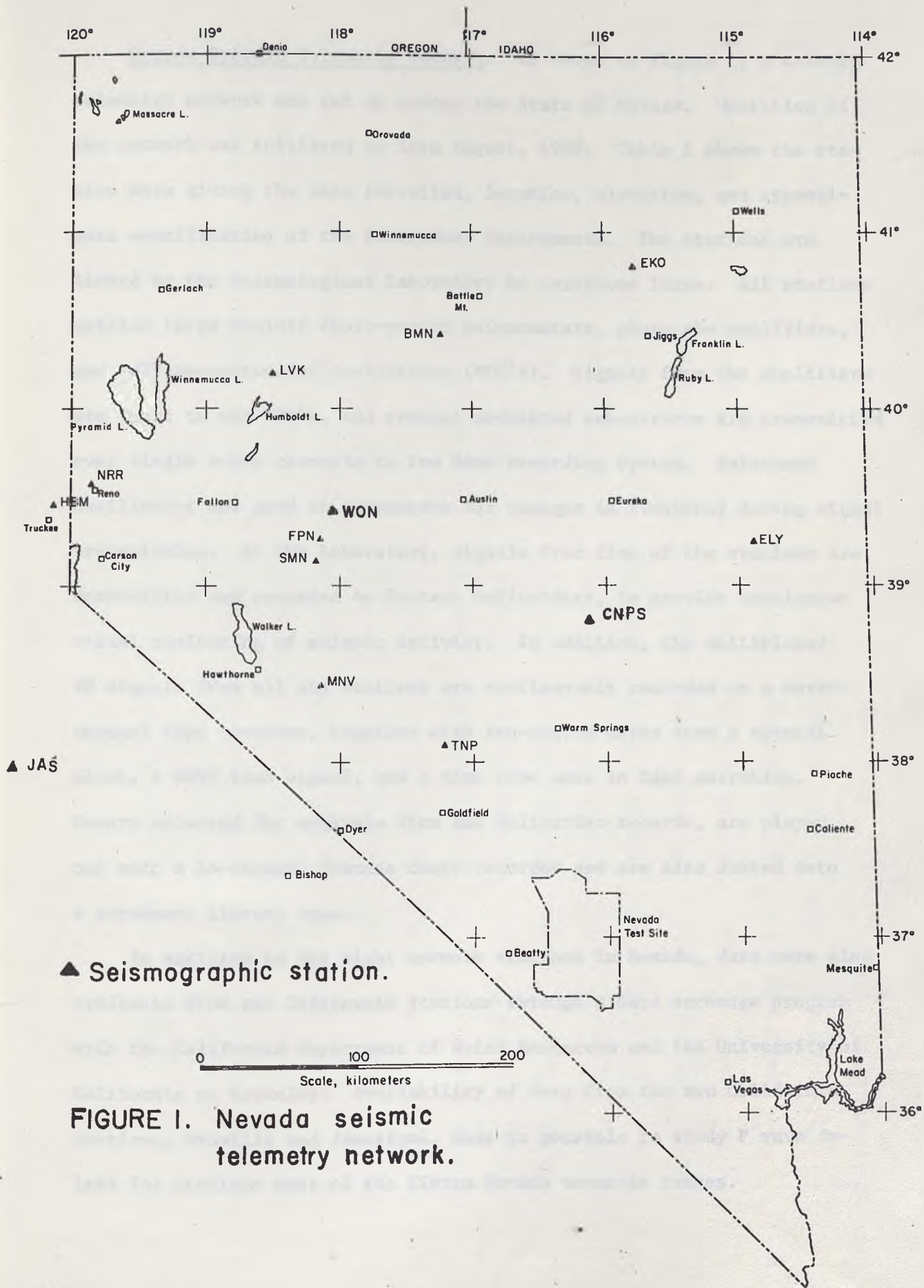
FIGURE 1. Nevada seismic telemetry network.

<u>Nevada Seismic Telemetry Network</u>. As shown on Figure 1, a seismic telemetry network was set up across the State of Nevada. Operation of the network was initiated in late August, 1969. Table 1 shows the station data giving the date installed, location, elevation, and approximate magnification of the individual instruments. The stations are linked to the Seismological Laboratory by telephone lines. All stations utilize large Benioff short-period seismometers, phototube amplifiers, and voltage-controlled oscillators (VCO's). Signals from the amplifiers are input to the VCO's, and several modulated subcarriers are transmitted over single voice channels to the Reno recording system. Reference oscillators are used to compensate for changes in frequency during signal transmission. At the Laboratory, signals from five of the stations are demodulated and recorded on Geotech Helicorders, to provide continuous visual monitoring of seismic activity. In addition, the multiplexed FM signals from all the stations are continuously recorded on a seven-channel tape recorder, together with ten-second marks from a crystal clock, a WWVB time signal, and a time code used in tape searching. Events selected for analysis from the Helicorder records, are played out onto a 16-channel Siemens chart recorder and are also dubbed onto a permanent library tape.

In addition to the eight network stations in Nevada, data were also available from two California stations through a data exchange program with the California Department of Water Resources and the University of California at Berkeley. Availability of data from the two California stations, Oroville and Jamestown, made it possible to study P wave delays for stations west of the Sierra Nevada mountain ranges.

Table 1. Station Data

Date Installed	Station Name	Code	Latitude Deg. N	Longitude Deg. W	Elev. Feet	Compo-nents	Approx. Magnifi-cation	Site Description
4/9/64	North Reno	NRR	39.5720	119.8490	5,360	NEZ	500K	Short mine drift 3 mi N of Reno
10/11/63	Tonopah	TNP	38.0820	117.2177	6,360	NEZ	700K	Mine drift 1 mi NE of Tonopah
9/2/69	Battle Mt.	BMN	40.4313	117.2217	4,920	NEZ	1,000K	Mine drift 22 mi SE of Battle Mt.
9/15/69	Ely*	ELY	39.2312	114.8999	6,670	Z	128K	In Murray Canyon, near Ely
10/20/69	Oroville	ORV	39.5555	121.5000	1,180	Z	--	Calif. Dept. of Water Resources
10/20/69	Jamestown	JAS	37.9467	120.4383	1,500	Z	--	Univ. of California, Berkeley
11/5/69	Lovelock	LVK	40.1870	118.5245	4,020	Z	400K	2 mi NW of Lovelock
11/12/69	Elko	EKO	40.8122	115.7760	5,300	Z	90K	1 mi SW of Elko
3/24/70	Hobart Mills	HBM	39.4017	120.1533	5,920	Z	600K	1 mi E of Hobart Mills, Calif.
3/8/70	Fairview Pk.	FPN	39.2488	118.1625	6,600	NEZ	2,000K	Temporary field installation
3/16/70	Slate Mt.	SMN	39.1105	118.1892	6,000	NEZ	2,000K	Temporary field installation
5/26/70	Mina	MNV	38.4328	118.1531	5,000	Z	--	Lawrence Radiation Laboratory
--	Wonder Mine	WON	39.4453	118.0503	6,000	Z	--	Temporary field installation
--	Hot Creek Valley	CNPS	38.7660	116.2037	--	Z	--	U.S. Geol. Surv. field installation

*Discontinued 6/22/70.

4

<u>Travel-time curves</u>. Before attempting locations of earthquakes in
the Nevada region, travel-time curves and velocities of various seismic
phases were determined using nuclear explosions detonated at the Nevada
Test Site in the southern part of the State. Nuclear explosions provide
a convenient source of energy for velocity determinations, since para-
meters like origin time, location, and depth of focus of the events are
known. The following phases were studied for the preparation of travel-
time curves:

(1) P_n, a compressional wave that has penetrated the earth's
     crust and propagates as a refracted wave along the crust-
     mantle boundary, at velocities of the upper-mantle rocks.
     The network stations covered a 110° range of azimuth extend-
     ing from about 280° - 30° with respect to the Nevada Test
     Site, which made possible a determination of the azimuthal
     dependence of P_n wave velocity from nuclear explosions alone.
     In addition, from events located by the network, interval
     velocities along different azimuths for several pairs of
     stations were also computed. Epicenters of earthquakes that
     were found to lie on a line with a pair of stations were used
     to determine the apparent P_n velocity between the two stations.

     A systematic variation of P_n velocity with azimuth can
     be explained as due to a dipping Mohorovicic discontinuity,
     and in the case of a plane dipping refractor, the amount and
     direction of the true dip can be determined. This will be
     discussed below in some detail.

(2) P*, a compressional wave that has penetrated through the upper
     layer of the crust and travels as a refracted wave in an

intermediate layer within the crust.

(3) P_g, a compressional wave that has penetrated the low-velocity sedimentary layer over the earth's crust and propagates as a refracted wave in the upper layer of the crust. P_g data on our records from nuclear explosions were rather scarce, or of poor quality. This was because the high energy content of the P_n wave train produced sufficient clipping to mask the P_g arrivals. P_g travel-times were studied mainly from events located by the network. The P* and S_g phases were treated similarly, and the scatter in the observations was fitted by least squares to a travel-time curve.

(4) S_g, a shear wave corresponding to the travel path of P_g above.

Previous work. A long-range program of seismic refraction measurements for the western United States was begun by the U.S. Geological Survey in 1961 as part of the Vela Uniform program. Altogether, more than 2,000 sites, extending from eastern Colorado to the California coastline and from central Idaho to the U.S.-Mexico border, were occupied to record seismic waves generated by underground nuclear and chemical explosions. Several results on travel-times and crustal structure have been reported since then, but are being continually reviewed and revised.

P_n velocity

The velocity of P_n over most of the Basin and Range province was found to be in the range 7.8 to 7.9 km/sec (Eaton, 1963; Pakiser and Hill, 1963; Roller and Healy, 1963; Ryall and Stuart, 1963). Eaton's profile from Fallon, Nevada, to Eureka, Nevada, gave an apparent P_n velocity of 7.62 km/sec. In the reversed direction from Eureka to Fallon, the apparent P_n velocity was 8.05 km/sec. Such variations in the

apparent velocity of P_n can be explained as the result of changes in crustal structure, with the crust-mantle boundary dipping toward the east, together with a slight decrease in upper-mantle velocity from the western margin towards the central portion of the Basin and Range. Eaton calculated the dip of the mantle from Fallon to Eureka to be 1.7° and a true P wave velocity of 7.82 km/sec. The crustal thickness at Eureka was determined to be 31.5 km.

Pakiser and Hill (1963) studied first arrivals of seismic waves generated by several underground nuclear explosions at the Nevada Test Site (NTS) and recorded along a line extending into southern Idaho. They found a P_n velocity of 7.84 km/sec and, assuming constant velocities and horizontal layers, the depth to the mantle in the neighborhood of the Test Site was determined to be about 28 km. They computed the thickness of the crust at Eureka, Nevada, to be 32 km which agrees well with the value of 31.5 km determined by Eaton (1963). In a later paper, Pakiser and Hill (1967) revised their value for the velocity and found it to be 7.9 km/sec for the same profile.

Roller and Healy (1963) reversed a refraction profile between Santa Monica Bay, California, and Lake Mead, Nevada, and found a crustal thickness of 30 km at Lake Mead. The upper mantle velocity was determined to be 7.8 km/sec.

A study by Ryall and Stuart (1963) of travel-times from NTS explosions to Ordway, Colorado, gave an apparent P_n velocity of 7.6 km/sec in the eastern part of the Basin and Range, and a crust increasing in thickness from about 25 km at NTS to about 42 km in the western part of the Colorado plateau.

P_g Velocity

The velocity of the crystalline crust underlying the near-surface sedimentary cover is approximately 6 km/sec. This velocity is constant to within ±0.1 km/sec throughout the Basin and Range and has been determined independently by several workers, for different sections of the Basin and Range province (Ryall and Jones, 1964). Eaton (1963) found a P_g velocity of 6.02 km/sec for the refraction line from Fallon to Eureka and a velocity of 5.92 km/sec for the reversed profile from Eureka to Fallon. However, the intercept-time of P_g varied from profile to profile, and this was explained as due to travel path through unusually thick accumulations of sedimentary deposits. Eaton also observed considerable scatter of P_g travel-times from point to point along a given profile. This was attributed to a wide variation in the thickness and velocity of near-surface rocks. Velocities of the near-surface rocks were divided into two groups, concentrated near 1.9 km/sec and 3.5 km/sec.

Ryall and Stuart (1963) found a P_g velocity of 6.0 km/sec for the eastern part of the Basin and Range province. This agrees with the velocity of 6.03 km/sec found by Pakiser and Hill (1963) for refraction lines from NTS to southern Idaho. The consistency in the value of P_g velocity for the Basin and Range is further exhibited by Roller and Healy (1963), who determined a value of 6.1 km/sec near Lake Mead, Nevada.

Intermediate P wave velocity

An intermediate layer of velocity 6.7 km/sec was found by Hill (1963) on reversed profiles, using chemical explosions from north of Elko, Nevada, to Boise, Idaho. Eaton (1963) and Roller and Healy (1963)

observed reflections which would require the presence of an intermediate velocity layer above the Mohorovicic discontinuity, and Eaton suggested a velocity of 6.6 km/sec for waves propagating in this layer. Ryall and Stuart (1963) recognized the presence of an intermediate layer of velocity 6.5 km/sec, in the Basin and Range province. Table 2 summarizes some of the important contributions to crustal structure in the Basin and Range province, by previous investigators.

Table 2. Summary of Crustal Structure in the Basin and Range Province (after Pakiser and Hill, 1963).

Investigators	Velocity of P_g, km/sec	Velocity of P_n, km/sec	Crustal Thickness km
Press, 1960	6.11	7.66	24
Berg, et al., 1960	5.73,6.33	7.59	25
Diment, et al., 1961	6.15	7.81	28
Pakiser and Hill, 1963	6.03	7.84	28
Eaton, 1963	6.02	7.82	22-31
Roller and Healy, 1963	6.1	7.8	30
Ryall and Stuart, 1963	6.0		25

Pakiser (1963) concluded that within the Basin and Range province, assuming a uniform P_n velocity, the variations in crustal thickness seem to be directly related to regional altitude above sea level.

Systematic variations in P_n velocity were first suggested by the work of Ryall (1962) and by Pakiser, et al (1962) of the U.S. Geological Survey. They found an azimuthal dependence for P_n velocity and attributed this to a dipping Mohorovicic discontinuity.

Herrin and Taggart (1962) found apparent P_n velocities ranging from about 7.6 to 7.9 km/sec across the State of Nevada. If it is assumed that the velocity of P_n does not vary systematically with distance from

the source, Herrin and Taggart concluded that the variations imply changes in state or composition of the uppermost mantle. The above range of velocities for P_n in Nevada was confirmed by the work of Archambeau, Flinn and Lambert (1969), with minor modifications. They also found rather abrupt changes in P_n velocity across physiographic province boundaries and attributed this to changes in the upper-mantle structure across such boundaries.

ANALYSIS AND RESULTS

From a preliminary knowledge of the P_g velocity derived from nu-
clear explosions, a computer program was developed in the Laboratory
for locating earthquakes in the Nevada region. This program also
determines the distance of the event from each station of the network
that recorded it, the event-to-station azimuth, P_g and S_g residuals for
each observation, the standard deviation of the solution, and the
travel-time for each phase observed by the network of stations.

Travel Time Curves

P_g Velocity. To determine the P_g travel-time equation, only those
earthquakes were used that were located within the network of seismo-
graphic stations already discussed. Observations from these earthquakes
produced clear P_g arrivals that could be read to an accuracy of about
0.1 to 0.2 seconds at all the recording stations. Also, the above
events within the network were those which had minimum location errors
that could be produced from incorrect velocity assumptions. The events
were located assuming a velocity and intercept time for P_g based on pre-
vious work and on explosion data from the Nevada Test Site. Velocity
and intercept-time were recalculated for P_g using travel-times from the
determined epicenters.

On the basis of observations extending to distances around 450 km
for P_g, a travel-time plot was constructed, which showed a feature
suggesting two possible velocities (Figure 2). The plot was slightly
curved up to 150-200 km beyond which points were observed to fall more
or less on a straight line.

Pg TRAVEL TIME
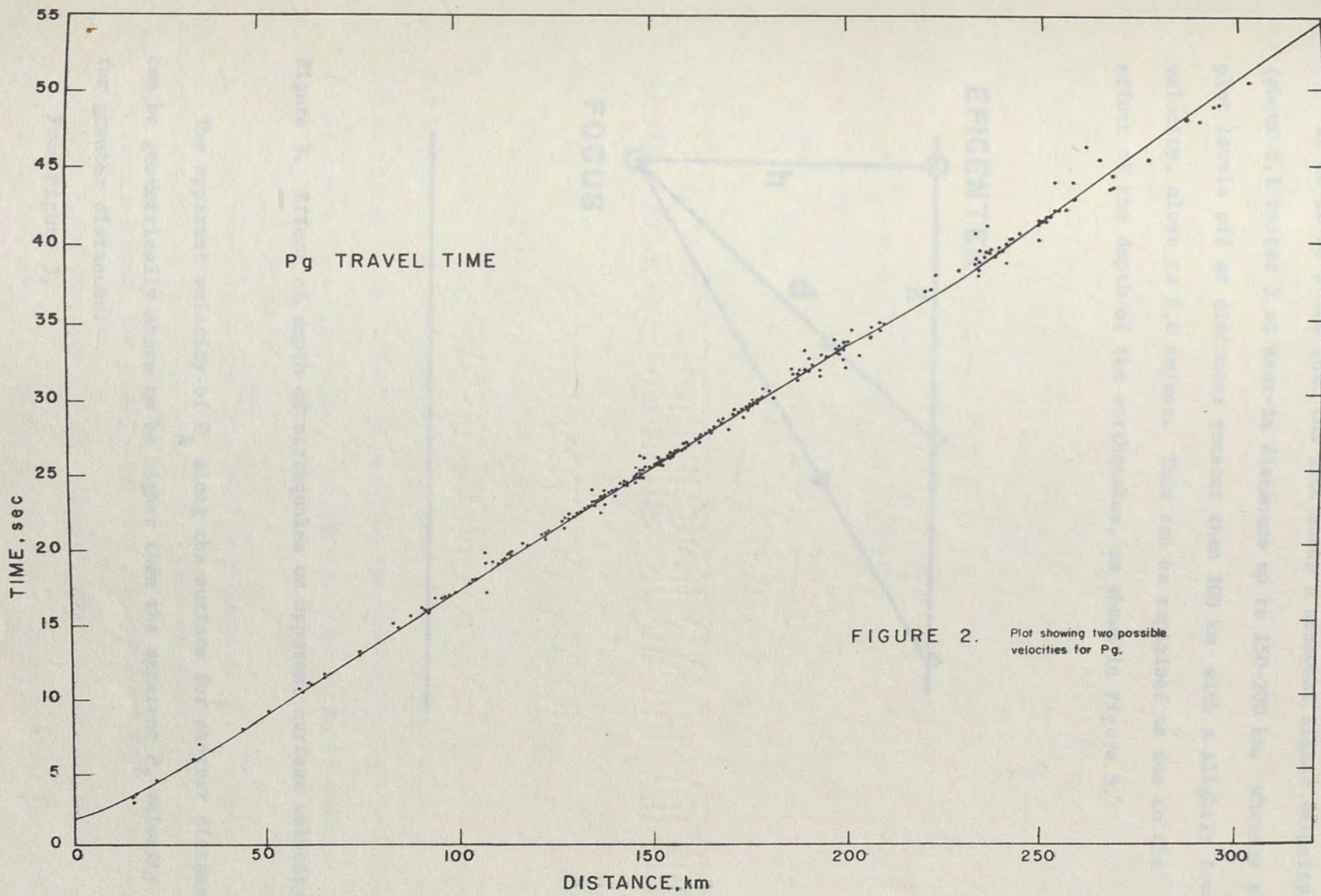
FIGURE 2.   Plot showing two possible
velocities for Pg.

It is to be noted that the plot shows a somewhat higher velocity (about 6.1 km/sec) at near-in distances up to 150-200 km, whereas the plot levels off at distances greater than 200 km with a slightly lower velocity, close to 6.0 km/sec. This can be explained as due to the effect of the depth of the earthquakes, as shown in Figure 3.

EPICENTER

FOCUS
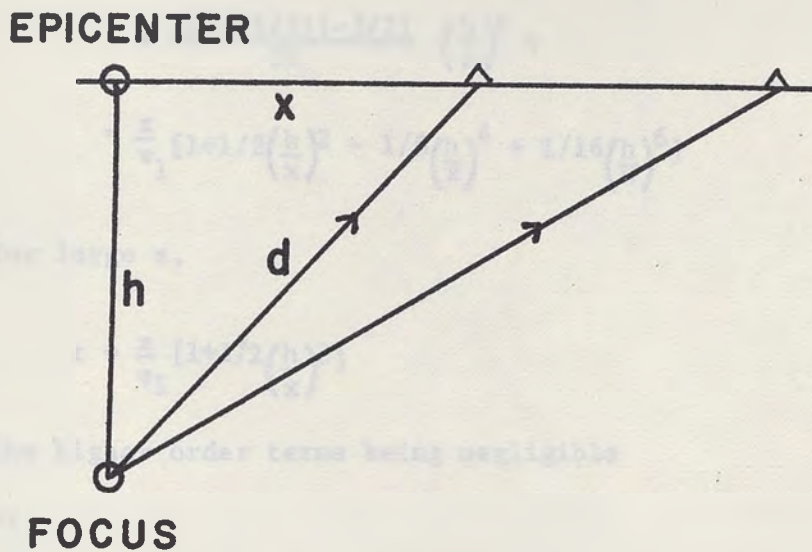
Figure 3. Effect of depth of earthquakes on apparent surface velocity.

The apparent velocity of P_g along the surface for shorter distances can be geometrically shown to be higher than the apparent P_g velocity for greater distances.

From Figure 3,

$$d = \sqrt{x^2 + h^2}$$

$$t = \frac{d}{v_1} = \frac{\sqrt{x^2 + h^2}}{v_1}$$

$$= \frac{x}{v_1} \left[1 + \left(\frac{h}{x}\right)^2\right]^{1/2}$$

$$= \frac{x}{v_1} \left[1 + 1/2\left(\frac{h}{x}\right)^2 + \frac{(1/2)(-1/2)}{2!} \left(\frac{h}{x}\right)^4 \right.$$

$$\left. + \frac{1/2(-1/2)(-3/2)}{3!} \left(\frac{h}{x}\right)^6 + \right.$$

$$= \frac{x}{v_1} \left[1 + 1/2\left(\frac{h}{x}\right)^2 - 1/8\left(\frac{h}{x}\right)^4 + 1/16\left(\frac{h}{x}\right)^6\right]$$

For large x,

$$t = \frac{x}{v_1} \left[1 + 1/2\left(\frac{h}{x}\right)^2\right]$$

the higher order terms being negligible

or,

$$v_1 = \frac{x}{t} \left[1 + \left(\frac{h}{x}\right)^2\right]$$

For increasing x, the term in the bracket becomes close to 1.0

and for large x, the effect of depth on the velocity becomes negligible,

at which point the true velocity in the layer approximates the apparent

surface velocity, $\frac{x}{t}$ km/sec.

Hence the travel-time data for P_g were divided into two parts, a)

for distances up to 200 km and b) for distances greater than 200 km.

Figure 4 shows the travel-time plot for the first case (distance

Δ <200 km) and includes 213 observations from earthquakes located

within the network. The least-squared travel-time equation was found to be:

Pg TRAVEL TIME

Δ < 200 km

$T_{Pg} = .9 + \triangle/6.13$

FIGURE 4.

DISTANCE, km

TIME, sec
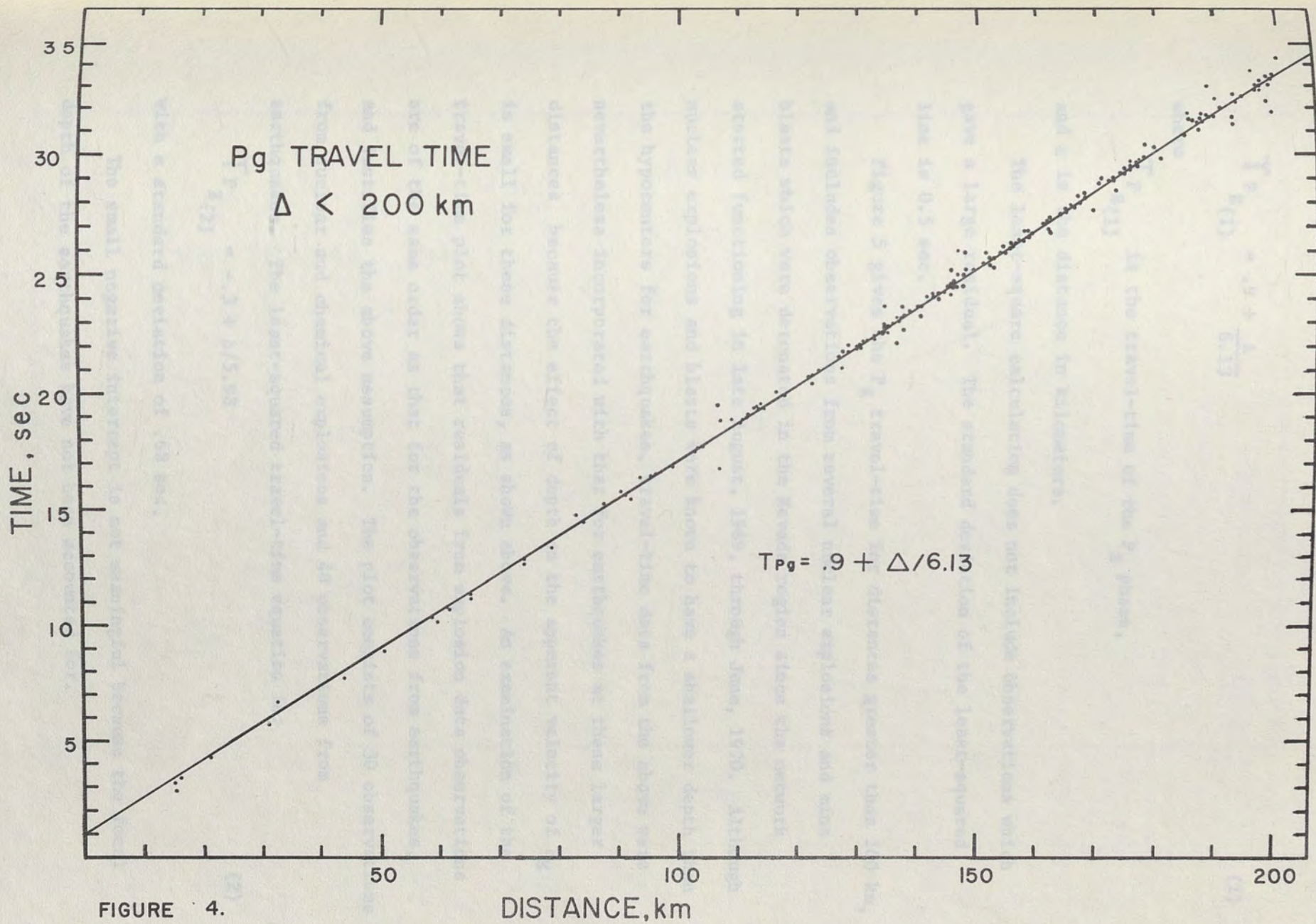
$$T_{P_{g_{(1)}}} = .9 + \frac{\Delta}{6.13} \qquad (1)$$

where

$T_{P_{g_{(1)}}}$ is the travel-time of the P_g phase,

and Δ is the distance in kilometers.

The least-square calculation does not include observations which gave a large residual. The standard deviation of the least-squared line is 0.5 sec.

Figure 5 gives the P_g travel-time for distances greater than 200 km, and includes observations from several nuclear explosions and mine blasts which were detonated in the Nevada region since the network started functioning in late August, 1969, through June, 1970. Although nuclear explosions and blasts were known to have a shallower depth than the hypocenters for earthquakes, travel-time data from the above were nevertheless incorporated with that for earthquakes at these larger distances because the effect of depth on the apparent velocity of P_g is small for these distances, as shown above. An examination of the travel-time plot shows that residuals from explosion data observations are of the same order as that for the observations from earthquakes, and justifies the above assumption. The plot consists of 30 observations from nuclear and chemical explosions and 40 observations from earthquakes. The least-squared travel-time equation is:

$$T_{P_{g_{(2)}}} = -.3 + \Delta/5.98 \qquad (2)$$

with a standard deviation of .68 sec.

The small negative intercept is not meaningful because the focal depth of the earthquakes have not been accounted for.

FIGURE 5.

The figure shows a graph titled "Pg TRAVEL TIME, $\Delta > 200$ km" with TIME, sec on the vertical axis (ranging 30 to 80) and DISTANCE, km on the horizontal axis (ranging 200 to 450). The line fit is given by $T_{Pg} = -.3 + \Delta/5.98$.
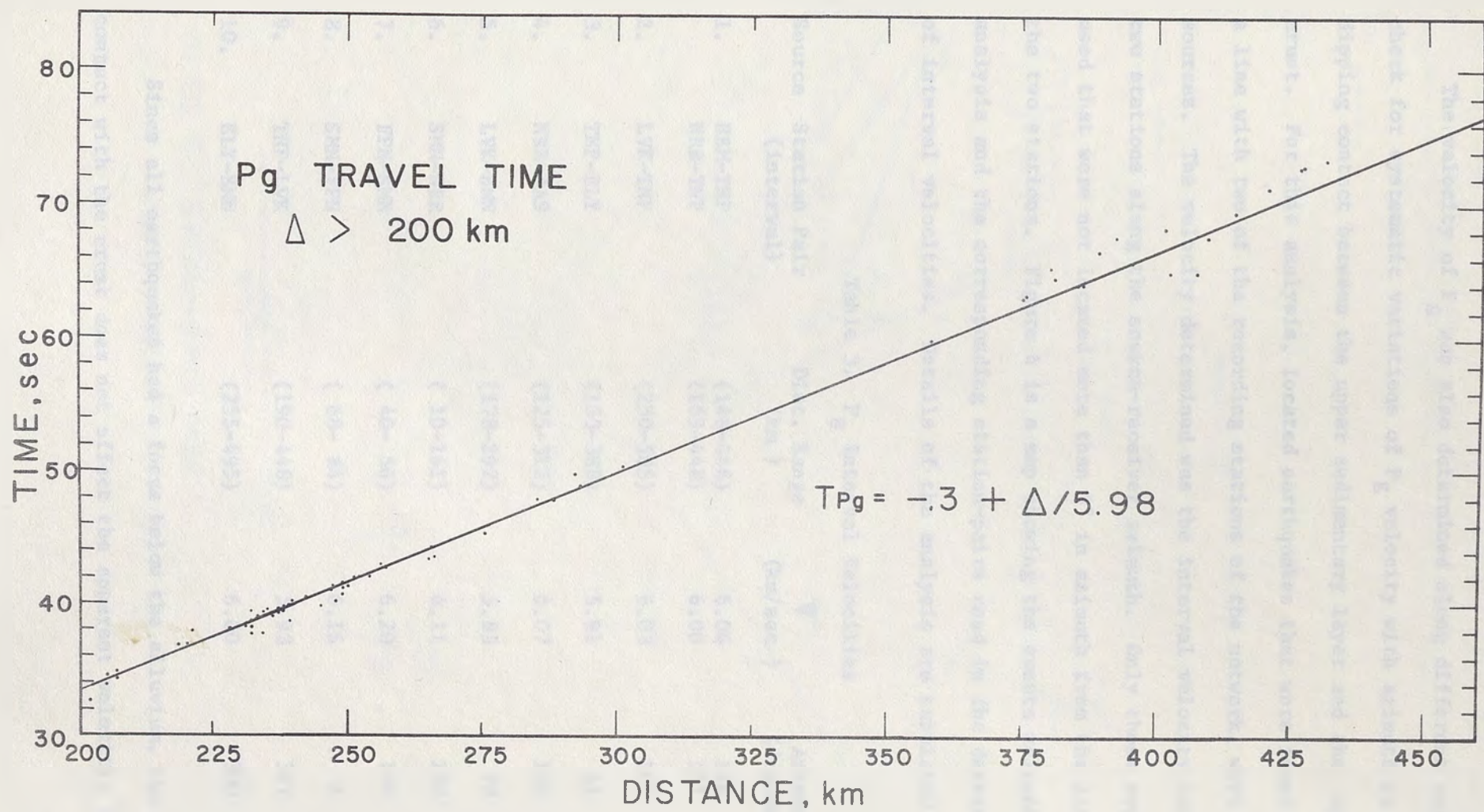
The velocity of P_g was also determined along different azimuths to check for systematic variations of P_g velocity with azimuth in case of a dipping contact between the upper sedimentary layer and the upper crust. For this analysis, located earthquakes that were found to be on a line with two of the recording stations of the network, were used as sources. The velocity determined was the interval velocity between the two stations along the source-receiver azimuth. Only those events were used that were not located more than 5° in azimuth from the line joining the two stations. Figure 6 is a map showing the events selected for analysis and the corresponding station-pairs used in the determination of interval velocities. Details of the analysis are tabulated in Table 3.

Table 3. P_g Interval Velocities

Source	Station Pair (interval)	Dist. Range (km)	$\overline{V}$ (km/sec)	Azimuth (degrees)
1.	HBM-TNP	(148-448)	6.06	126
	NRR-TNP	(169-448)	6.00	121
2.	LVK-TNP	(250-505)	6.03	165
3.	TNP-ELY	(153-388)	5.91	61
4.	NRR-JAS	(125-312)	6.07	190
5.	LVK-BMN	(178-292)	5.83	78
6.	SMN-NRR	(10-161)	6.11	288
7.	FPN-SMN	(40- 56)	6.20	190
8.	SMN-FPN	(68- 84)	6.16	2
9.	TNP-LVK	(190-448)	5.93	327
10.	ELY-BMN	(255-495)	6.00	300

Since all earthquakes had a focus below the alluvium, the alluvium contact with the crust does not affect the apparent velocity, $\overline{V}$.
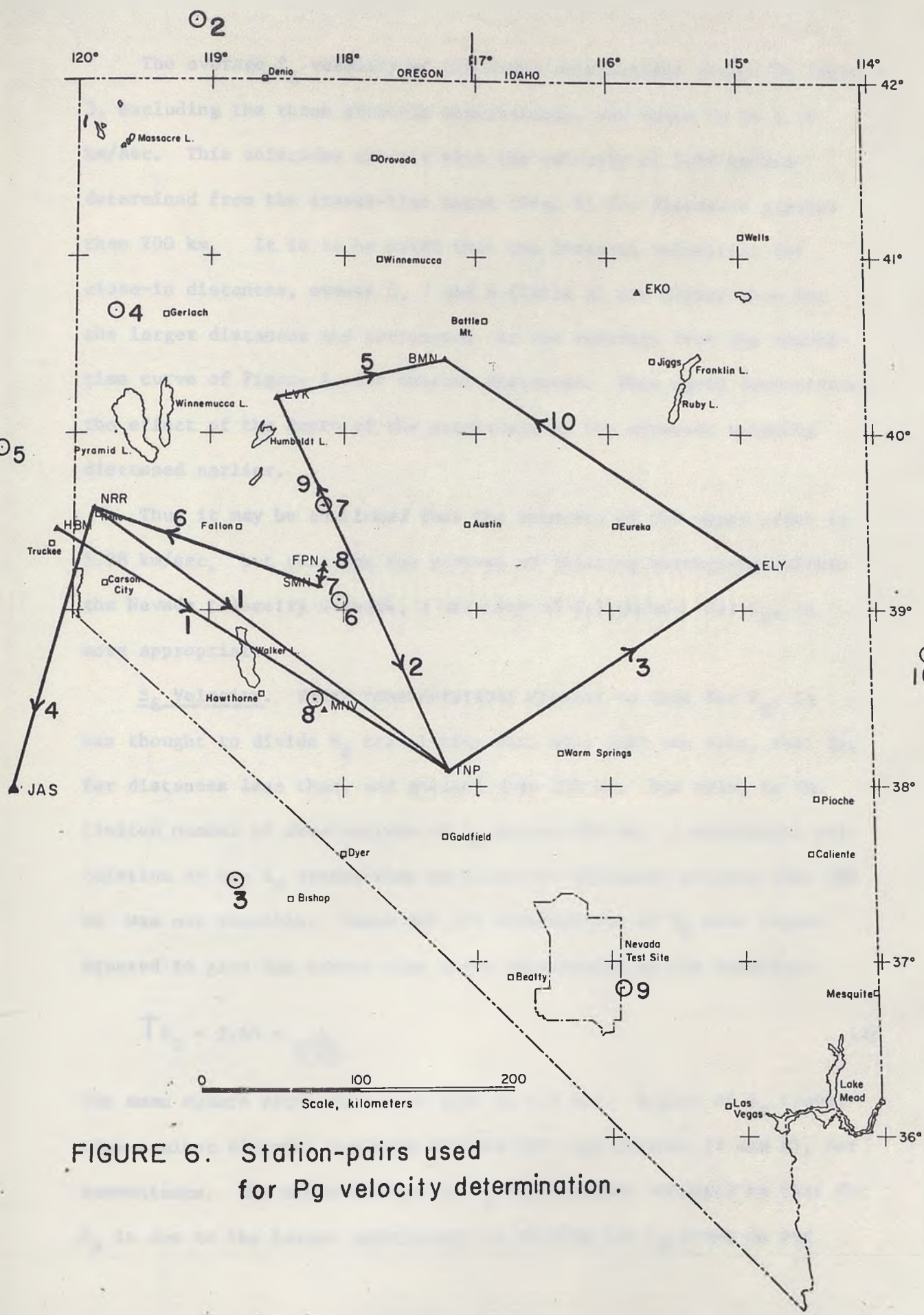
FIGURE 6. Station-pairs used
for Pg velocity determination.

The average P_g velocity of the eight observations listed in Table 3, excluding the three close-in observations, was found to be 5.98 km/sec. This coincides exactly with the velocity of 5.98 km/sec determined from the travel-time curve (Fig. 5) for distances greater than 200 km.   It is to be noted that the interval velocities for close-in distances, events 6, 7 and 8 (Table 3) are higher than for the larger distances and correspond to the velocity from the travel-time curve of Figure 4, for shorter distances. This again demonstrates the effect of the depth of the earthquake on the apparent velocity discussed earlier.

Thus it may be concluded that the velocity of the upper crust is 5.98 km/sec, but that for the purpose of locating earthquakes within the Nevada telemetry network, a velocity of 6.1 km/sec for P_g, is more appropriate.

$\underline{S_g \text{ Velocity}}$.   Under considerations similar to that for P_g, it was thought to divide S_g travel-time data also into two sets, that is, for distances less than, and greater than 200 km. But owing to the limited number of observations of S_g beyond 200 km, a meaningful calculation of the S_g travel-time equation for distances greater than 200 km was not feasible. Hence all 175 observations of S_g were least-squared to give one travel-time curve represented by the equation:

$$T_{S_g} = 2.65 + \frac{\Delta}{3.62} \tag{3}$$

The mean square error from this line is 0.9 sec. A plot of S_g travel-time against distance has been divided into two Figures (7 and 8), for convenience. The wider scatter in S_g observations compared to that for P_g is due to the larger uncertainty in picking the S_g phase on our

Sg TRAVEL TIME
Δ < 150 km

$T_{sg} = 2.65 + \Delta/3.62$

FIGURE 7.

Sg TRAVEL TIME

$\Delta > 150$ km

$T_{sg} = 2.65 + \Delta/3.62$
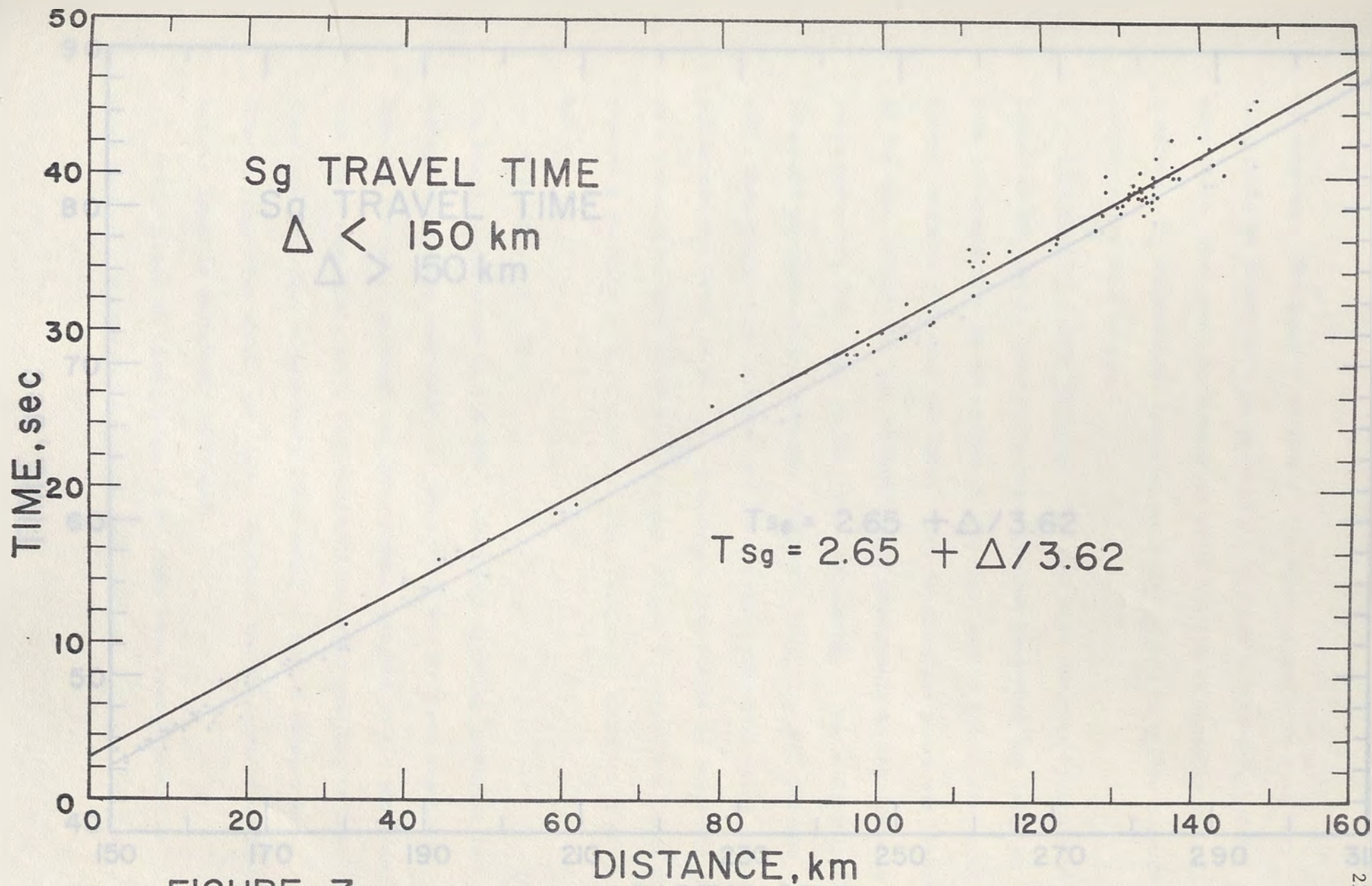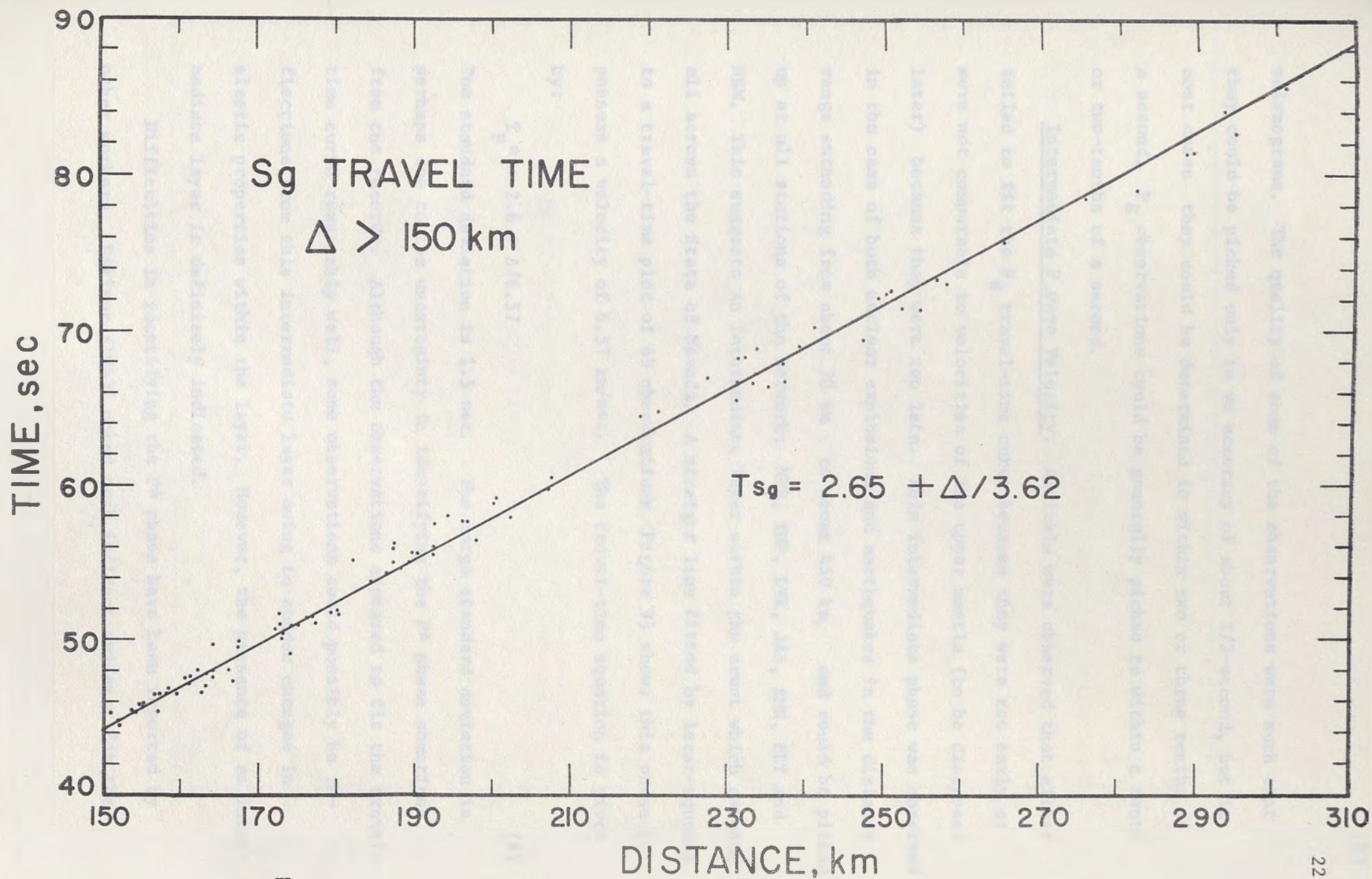
FIGURE 8.

seismograms. The quality of some of the observations were such that
they could be picked only to an accuracy of about 1/2-second, but in
most cases they could be determined to within two or three tenths of
a second. P_g observations could be generally picked to within a tenth
or two-tenths of a second.

Intermediate P .wave Velocity. Arrivals were observed that either
failed to fit the P_g travel-time curve because they were too early or
were not comparable to velocities of the upper mantle (to be discussed
later) because they were too late. This intermediate phase was observed
in the case of both nuclear explosions and earthquakes in the distance
range extending from about 70 km to about 450 km, and could be picked
up at all stations of the network: NRR, TNP, LVK, JAS, BMN, ELY and
HBM. This suggests an intermediate layer within the crust which extends
all across the State of Nevada. A straight line fitted by least-squares
to a travel-time plot of 45 observations (Figure 9) shows this phase to
possess a velocity of 6.57 km/sec. The travel-time equation is given
by:

$$T_p{}^* = 2.6 + \Delta/6.57 \tag{4}$$

The standard deviation is 1.5 sec. The large standard deviation is
perhaps due to the uncertainty in identifying the P* phase sometimes,
from the records. Although the observations appeared to fit the travel-
time curve reasonably well, some observations could possibly be re-
flections from this intermediate layer owing to sudden changes in
elastic properties within the layer. However, the presence of an inter-
mediate layer is definitely indicated.

Difficulties in identifying the P* phase have been reported by
other workers. Pakiser (1963) noted much indirect evidence for the

P* TRAVEL TIME

$T_{P^*} = 2.6 + \triangle/6.57$
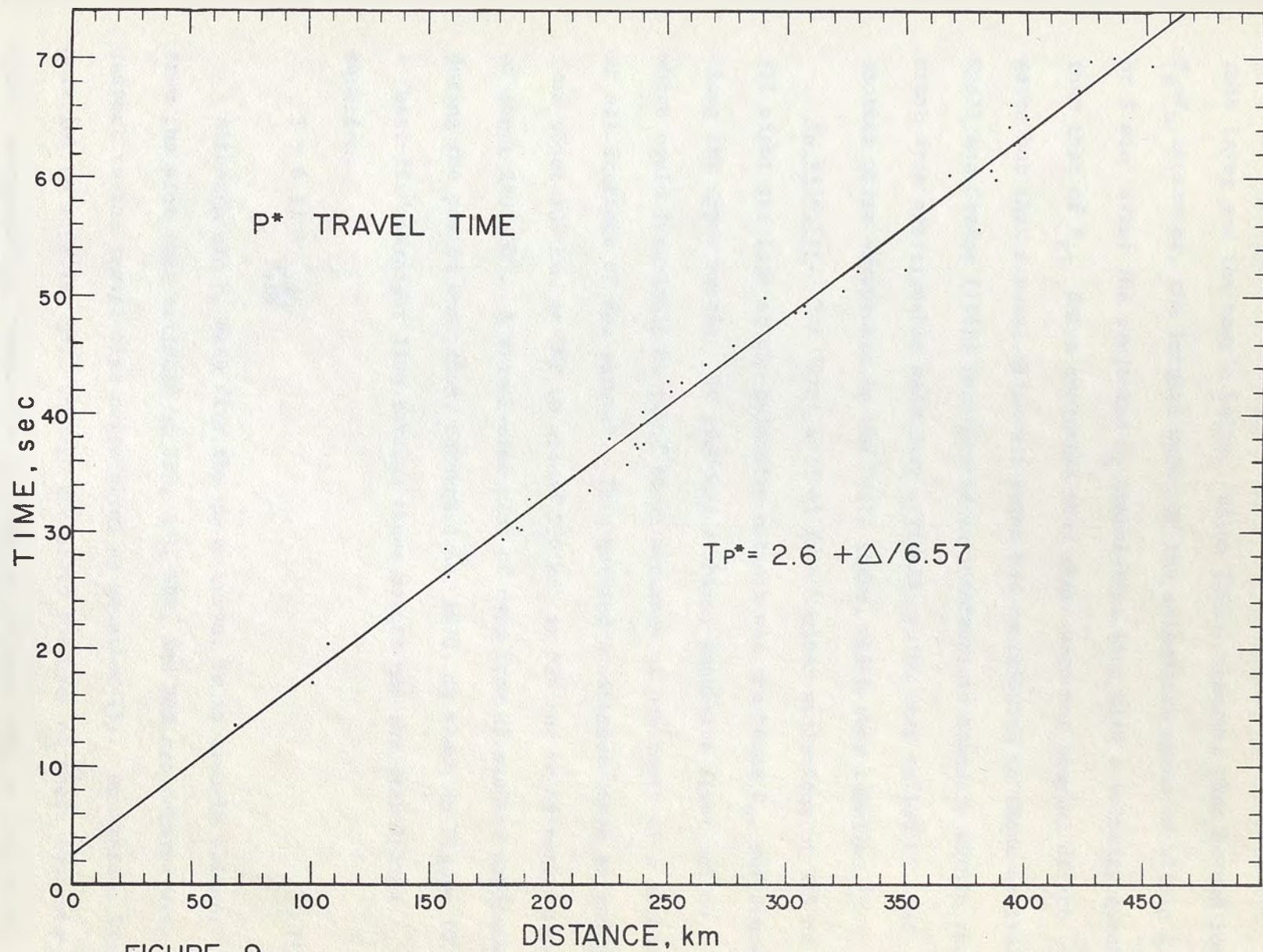
FIGURE 9.

presence of this layer, but could make no firm conclusions as to the nature of the boundary or transition zone with the upper crust above this layer and the mantle below. Eaton (1963) observed that beyond the P_g-P_n crossover, the largest waves on the seismogram appeared within 1 or 2 sec after the projected P_g travel-time line with a velocity greater than that of P_g. Eaton suggested that these were not simple, direct waves but that several different paths had contributed to these arrivals. Ryall and Stuart (1963) interpreted an intermediate boundary within the crust from questionable secondary arrivals, which they called P*, and another phase asymptotic to the P*(?) curve, which they labelled $\overline{P}$.

P_n Velocity. The first arrival from nuclear explosions at NTS at all eight stations of the telemetry network was the phase P_n, refracted along the upper mantle. It produced a sharp, impulsive first motion which could invariably be timed to an accuracy of one-tenth of a second, at all stations of the network. This covered a distance range extending from about 130 km at TNP to around 550 km at ORV and an azimuth range of about 280°-30°. A travel-time plot of data from 25 nuclear explosions during the period Oct. 1969, through June, 1970, is shown in Figure 10. A "best-fit" straight line through these points has the travel-time equation:

$$T = 6.51 + \frac{\Delta}{7.89} \tag{5}$$

Although all P_n data fits the above curve, it is clearly evident from the plot that arrivals at ORV, JAS, NRR, and HBM are delayed with respect to the travel-time curve given by equation (5). An average line, parallel to equation (5), through the plots for each of these four stations, respectively, shows that arrivals at ORV and JAS are delayed by

Pn TRAVEL TIME
FROM NUCLEAR EXPLOSIONS

$$T_{Pn} = 6.51 + \Delta/7.89$$

FIGURE 10.

△   JAS observations
⊙   NRR   "
□   HBM   "
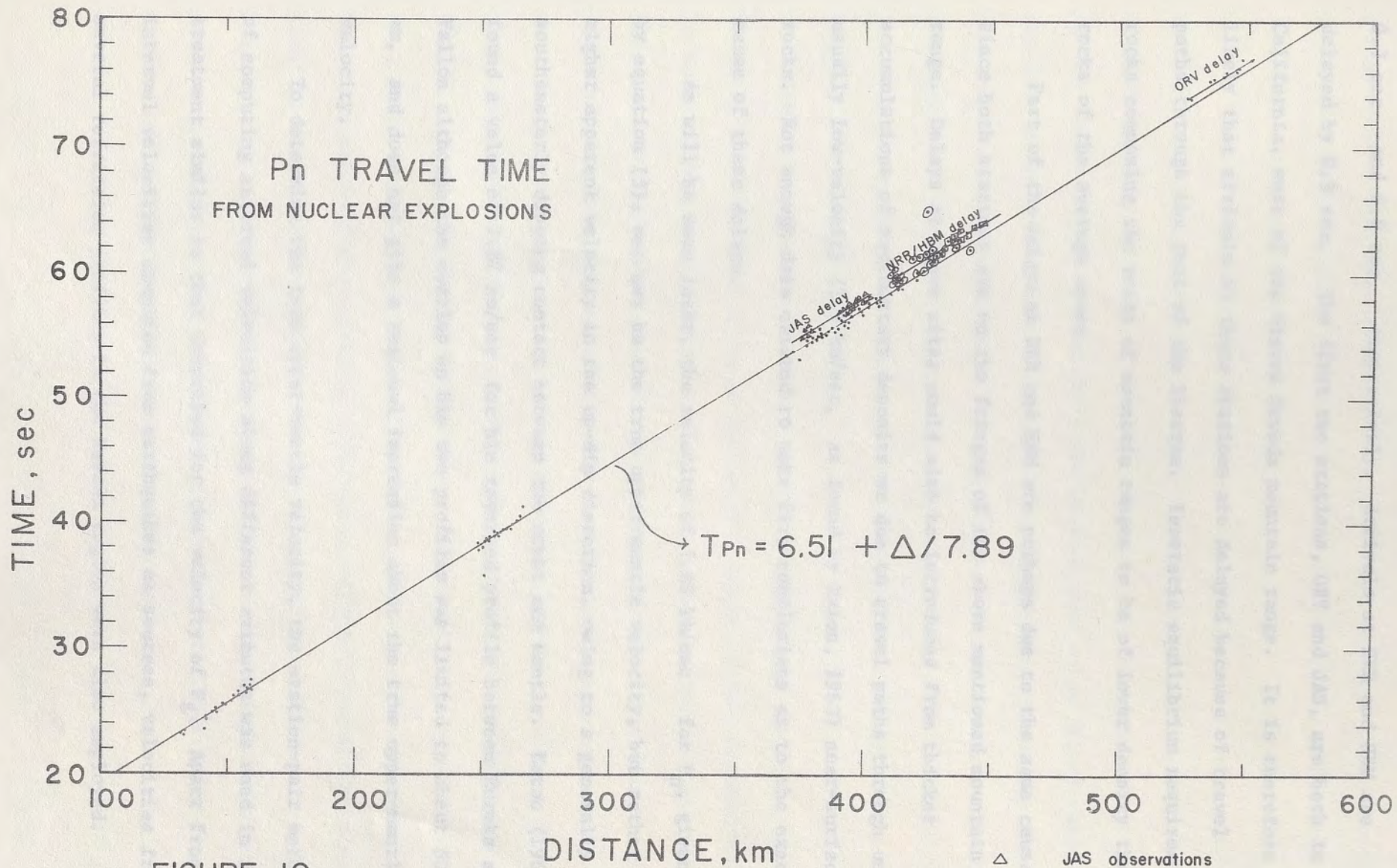
0.7 sec and 0.8 sec, respectively. Arrivals at NRR and HBM are

delayed by 0.9 sec.   The first two stations, ORV and JAS, are both in

California, west of the Sierra Nevada mountain range. It is therefore

likely that arrivals at these stations are delayed because of travel

paths through the root of the Sierras. Isostatic equilibrium requires

rocks composing the roots of mountain ranges to be of lower density than

rocks of the average crust.

Part of the delays at NRR and HBM are perhaps due to the same cause,

since both stations are on the fringes of the above mentioned mountain

range. Delays at these sites could also be introduced from thicker

accumulations of sedimentary deposits or due to travel paths through un-

usually low-velocity (1.9 km/sec, as found by Eaton, 1963) near-surface

rocks. Not enough data existed to make firm conclusions as to the exact

cause of these delays.

As will be seen later, the velocity of 7.89 km/sec for P_n, given

by equation (5), may not be the true upper-mantle velocity, but rather a

higher apparent velocity in the up-dip direction, owing to a generally

southeasterly dipping contact between the crust and mantle. Eaton (1963)

found a value of 7.82 km/sec for his reversed profile between Eureka and

Fallon although the overlap on his two profiles was limited to about 50

km, and does not give a regional impression about the true upper-mantle

velocity.

To determine the true upper-mantle velocity, the station-pair method

of computing interval velocities along different azimuths was used in a

treatment similar to that described for the velocity of P_g. Apart from

interval velocities computed from earthquakes as sources, velocities from

several refraction profiles in the Nevada region were also employed.

Altogether 14 observations of interval velocities and velocities from refraction profiles along different azimuths were available and distributed over almost the entire State.

A plot of all the available observations of apparent P_n velocity as a function of shot-receiver azimuth showed a systematic relationship between apparent velocity and azimuth. However, the standard deviation of the individual plots from the least-squared sine curve fitted through the points was rather large. This was because the area covered by all the observations was too large and suggests that the structure could be different from region to region within this area.

For the purposes of this study, the state was divided into three regions (Figure 11).

Region I covers the southwest part of the State and overlaps slightly with Region II so as to include the central Nevada seismic zone in both regions, events from which led to some observations of interval velocity. Altogehter, 6 observations of apparent velocities along various azimuths were selected for this region, including a refraction profile (Figure 12), from the nuclear explosion "STINGER' of March 22, 1968, and a velocity for western Nevada derived from the Truckee, California, earthquake sequence of September, 1966 (Ryall, et al, 1968).

Table 4 lists the 6 observations showing the apparent velocities and their corresponding azimuths. The map on Figure 13 shows the locations of the various profiles and their corresponding sources, and Figure 14 is a plot of the apparent velocities as a function of the source-receiver azimuth. Calculation of apparent velocities takes into account the delays, if any, at the respective stations.

120° 119° 118° OREGON 117° IDAHO 116° 115° 114° 42°

Denio

Massacre L.

□Orovada

REGION II □Winnemucca 41° REGION III □Wells

▲EKO

□Gerlach Battle M

BMN ▲ □Jiggs Franklin L.

Winnemucca L. ▲LVK Ruby L.

Pyramid L. Humboldt L. 40°

NRR Reno

▲HBM Fallon □ Austin □Eureka

Truckee

FPN▲ ▲ELY

□Carson City SMN ▲ 39°

Walker L.

Hawthorne□ REGION I □Warm Springs

▲MNV

▲TNP 38° □Pioche

□Goldfield □Caliente

□Dyer

□Bishop 37°

Nevada Test Site Mesquite

□Beatty

Lake Mead

0   100   200 □Las Vegas 36°

Scale, kilometers

FIGURE II. The three regions.
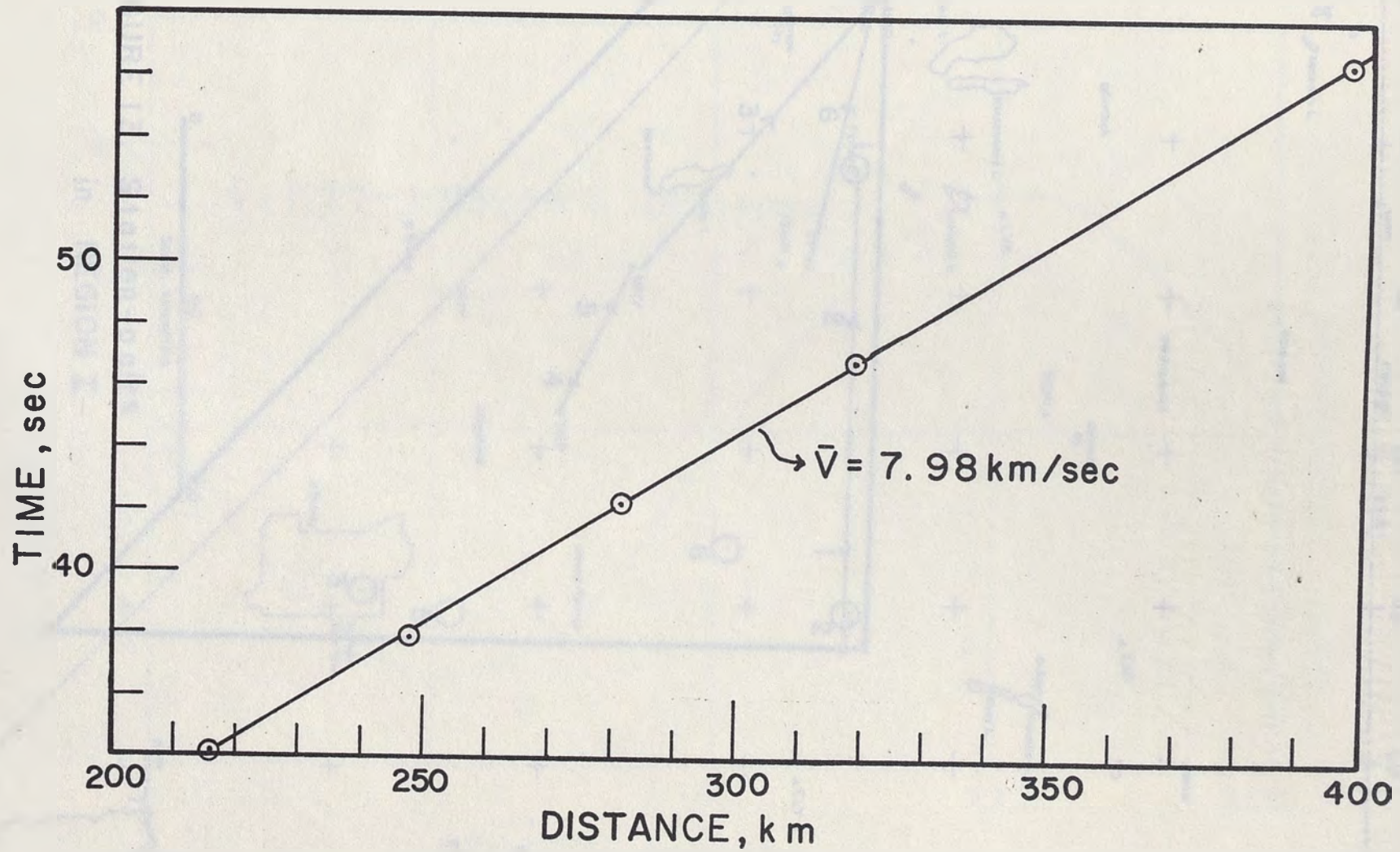
FIGURE 12. "Stinger" refraction profile.
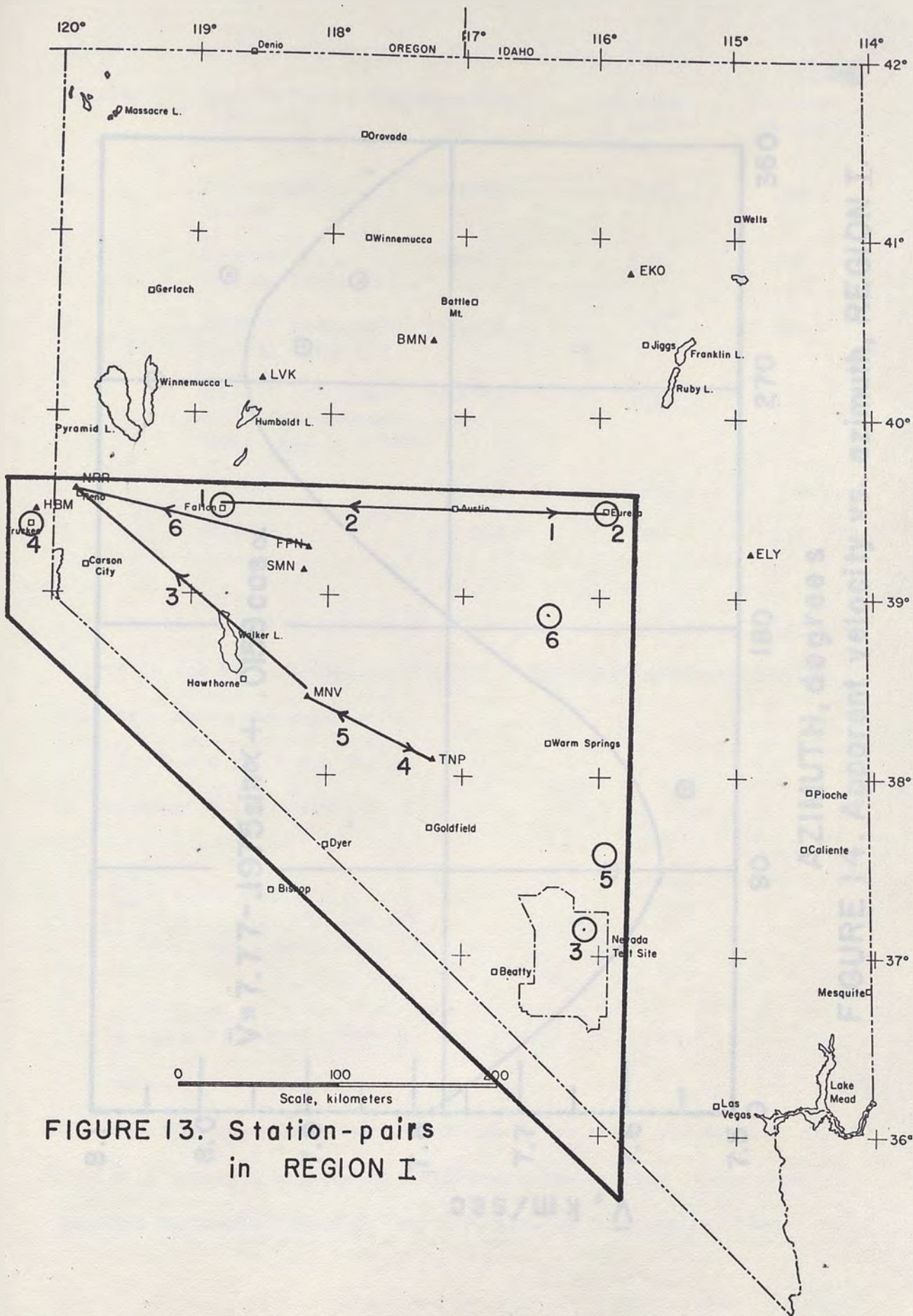
FIGURE 13. Station-pairs in REGION I

$$\bar{V} = 7.77 - .1975\sin\alpha + .0158\cos\alpha$$
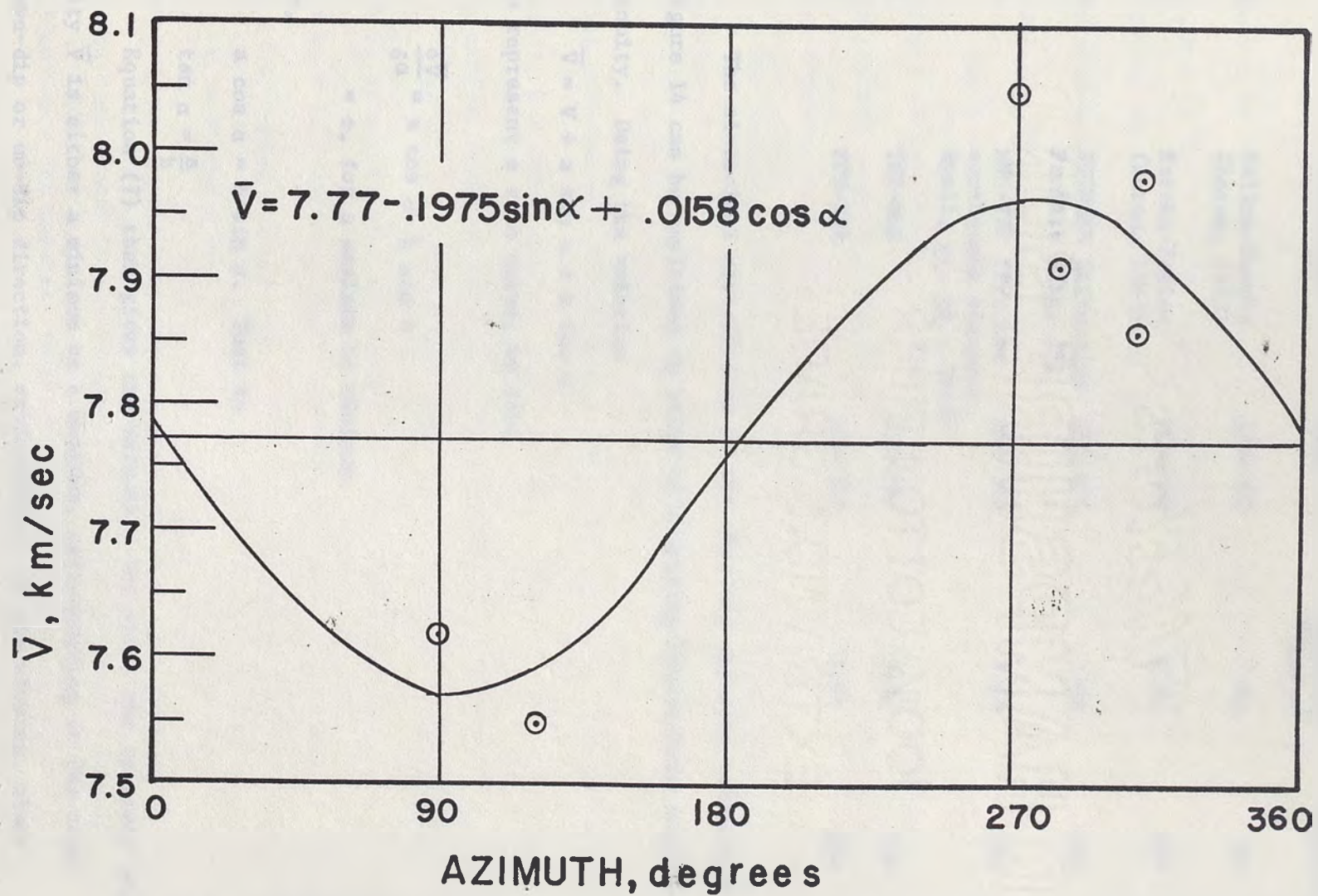
AZIMUTH, degrees

FIGURE 14. Apparent velocity vs. azimuth, REGION I.

Table 4.   Apparent P_n Velocities for Region I

Source	Station Pair (interval)	Distance Range (km)	Apparent Velocity $\overline{V}$(km/sec)	Azimuth (degrees)
1	Fallon-Eureka (Eaton, 1963)	125-300	7.62	90
2	Eureka-Fallon (Eaton, 1963)	150-300	8.05	270
3	STINGER Refraction Profile (fig. 15)	215-400	7.98	310
4	MNN-TNP (Truckee earthquake sequence, Ryall, et. al., 1968)	206-300	7.55	121
5	TNP-MNN	138-227	7.86	308
6	FPN-NRR	158-307	7.91	284

The sinusoidal distribution of the observed apparent velocities in Figure 14 can be explained in terms of a dipping Mohorovicic discontinuity. Using the relation

$$\overline{V} = V + a \sin \alpha + b \cos \alpha \qquad (6)$$

to represent a sine curve, we find

$$\frac{\delta \overline{V}}{\delta \alpha} = a \cos \alpha - b \sin \alpha$$

$$= o, \text{ for a maximum or minimum.}$$

Or,

a cos α = b sin α.   That is

$$\tan \alpha = \frac{a}{b} \qquad (7)$$

Equation (7) then gives the azimuth α for which the apparent velocity $\overline{V}$ is either a minimum or a maximum, corresponding to the true down-dip or up-dip direction, respectively, of the sloping, plane

refractor. The apparent velocity of refracted waves in the case of a
dipping interface can be expressed by the equation

$$\bar{v}_2 = v_1/\text{Sin} (i_c + \beta) \qquad (8)$$

where v_1 is the velocity in the layer above the interface; $i_c = \text{Sin}^{-1}$
(v_1/v_2) is the critical angle of refraction for the waves; v_2 is the true
velocity in the marker layer; and β is the apparent dip of the plane in
the shot-receiver direction. β is related to δ, the true dip of the
plane, by the relation

$$\text{Sin } \beta = \text{Sin } \delta \text{ Cos } \gamma \qquad (9)$$

where γ is the azimuth between the direction of dip and the direction of
the profile under consideration. So that if the profile is along the
true down-dip direction, $\gamma = 0$, and $\beta = \delta$.

The least-square sine curve of Figure 14 can be expressed by the
relation

$$\bar{V} = 7.77 - .1975 \text{ Sin } \alpha + .0158 \text{ Cos } \alpha \qquad (10)$$

Using calculations from equations (7), (8), and (9), substituting for a =
-.1975, b = .0158 and the true refractor velocity v_2 = 7.77 km/sec, a refract-
ing horizon is found which dips by an amount 1°52' in direction S85°26'E.

From the travel-time curve for the nuclear test STINGER (Figure 12),
the P_n intercept time at the test site is 7.02 sec. If v_1 = 6.0 km/sec
and v_2 = 7.77 km/sec, depth corresponding to this intercept is about
33.1 km, using the relation

$$T_i = 2h \text{ Cos } i_c/v_1 \qquad (11)$$

where T_i is the intercept time in seconds; h is the depth in km from
the surface normal to the refractor; i_c is the critical angle of
refraction. The apparent velocity of 7.98 km/sec for the STINGER
event along azimuth 310°, indicates that the crust thins towards NRR

with a dip of the base = 1°48' (apparent dip along 310°, calculated from equation (8). Over a distance of 390 km, this dip would result in a thinning of about 12.2 km from the equation

$$\Delta h = Tan \; \beta x \; distance \qquad (12)$$

where Δh is the difference in thickness, and β is the apparent dip. Hence crustal thickness at NRR should be in the vicinity of 21 km.

The above profile also passes through the station site at TNP, at a distance of 115 km from the shot. For this distance, crustal thinning is of the order of 3.6 km. Hence depth to the crust-mantle interface beneath TNP should be 29.5 km.

Using the above method of calculating apparent dips from apparent velocities, differences in crustal thickness between station pairs can be determined. If the absolute depth to the discontinuity at one of the stations is known, the depth at the other can be calculated. Table 5 lists the apparent dips and differences in thickness for the intervals used. The absolute value of crustal thickness for each site is given in Table 6, based on the value of 33.1 km calculated from the intercept time of the STINGER event. The only check available for this value of the depth at NTS is from previous work. Depths ranging from 26-34 km have been reported by several workers.

Pakiser and Hill (1963) initially found a value of 28 km for the crustal thickness at NTS from their refraction profile from NTS to Boise, Idaho. In a later study for the same profile (Pakiser and Hill, 1967), they revised their travel-time expression to

$$T = 6.38 + \Delta/7.90$$

which yields a 30 km depth to the refracting horizon beneath NTS. The true intercept time for NTS could perhaps be still larger (which would

Table 5. Apparent dips and Δh for Region I.
A negative apparent dip implies travel path
up-dip; positive dip for a profile in the
down-dip direction.

Station-Pair (interval)	Apparent Dip, β	Distance (km)	Diff. in Crustal Thickness, Δh (km)
NTS–NRR	–1°48'	390	12.2
NTS–TNP	–1°48'	115	3.6
TNP–MNV	–0°47'	89	1.2
FPN–NRR	–1°13'	149	3.2

Table 6. Crustal thickness based on value
of 33.1 km for thickness at NTS.

Site	Crustal Thickness (km)
NTS	33.1
NRR	20.9
TNP	29.5
MNV	28.3
FPN	24.5
Fallon (Eaton, 1963)	22
Eureka (Eaton, 1963)	31.5

give a still larger depth), because the line through their travel-times
is not an average least-square fitting, but rather connecting the earli-
est arrivals, so that they could examine possible delays.

An analytical solution by Knopoff and Teng (1965) for part of
Pakiser and Hill's (1963) data, shows the P_n travel-time to be

$$T = 6.7 + \Delta/7.87$$

This intercept would yield a thickness of the crust at NTS to be 31 km.

It is to be noted that an imperfect knowledge of the velocity-depth
relations in the crust could introduce uncertainties in crustal thick-
ness of the order of 5 km (Pakiser, 1963).

The value of 22 km for the crustal thickness at Fallon, about 90 km east of NRR, determined from a completely independent study (Eaton, 1963), is in general agreement with an increase of crustal thickness in an easterly direction from NRR.

Region II is the northwest part of the State and contains 7 observations of interval velocities from different sources. The various station-pair intervals and their corresponding sources are shown on a map in Figure 15; the azimuths, apparent velocities, and distance ranges for the various profiles are listed in Table 7; and the apparent velocities for the region are plotted as a function of the source-receiver azimuth on Figure 16.

Table 7.   Apparent P_n Velocities for Region II.

Source	Station-Pair (interval)	Distance Range (km)	App. Velocity $\overline{V}$ (km/sec)	Azimuth (degrees)
1	FPN–NRR	158–307	7.91	284
2	WON–SMN	145–185	7.86	200
3	Eureka–Fallon (Eaton, 1963)	150–300	8.05	270
4	BMN–LVK	155–270	7.80	262
5	LVK–BMN	268–379	7.71	91
6	Adel Refraction Line (See t–t curve, Fig. 17)	440–550	7.71	330
7	WON–BMN	140–263	7.78	21

The least-square sine curve drawn through the points in Figure 16 can be expressed by the equation

$$\overline{V} = 7.84 - .1650 \, \text{Sin} \, \alpha + .0048 \, \text{Cos} \, \alpha \tag{13}$$
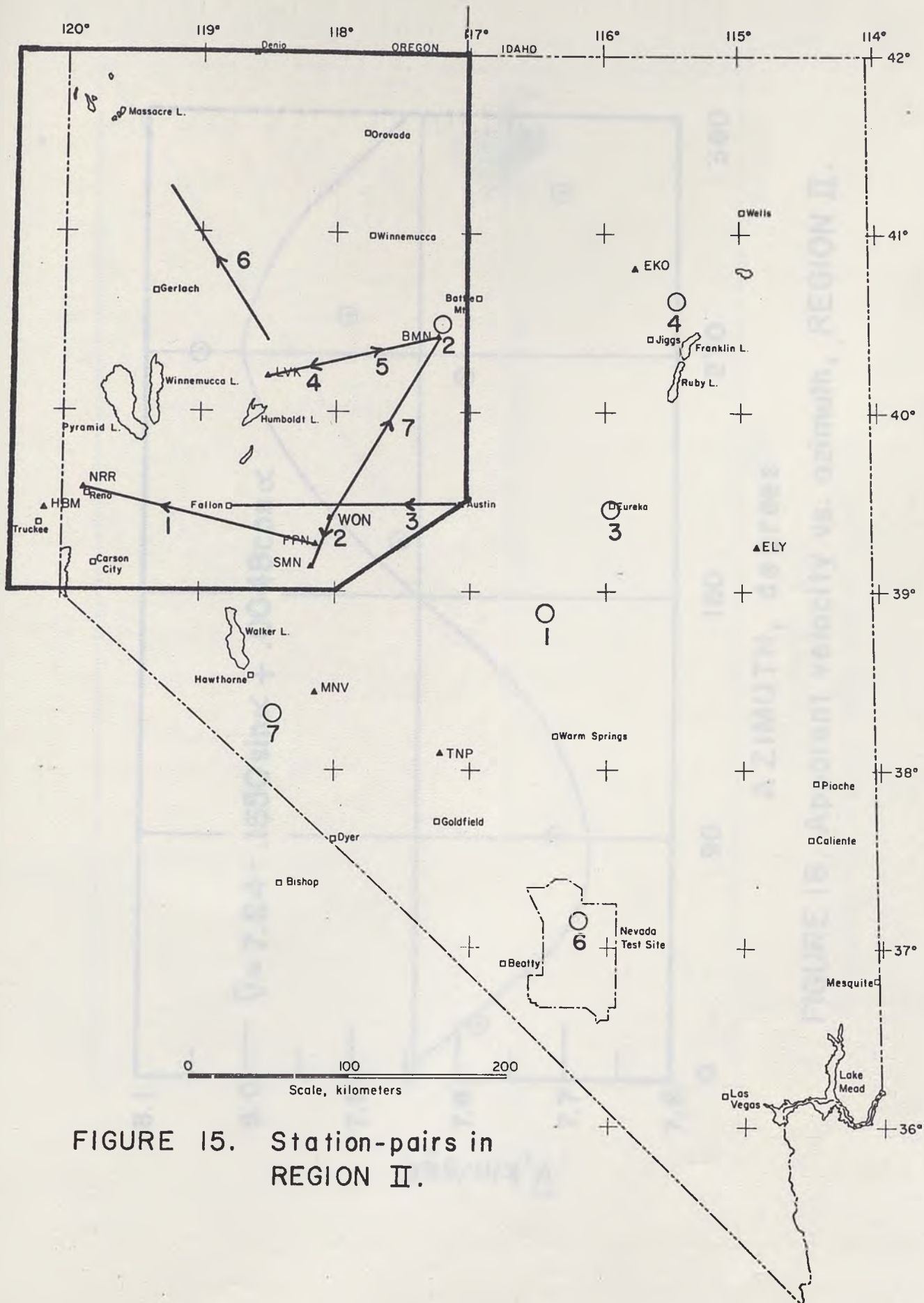
FIGURE 15. Station-pairs in REGION II.

$$\bar{V} = 7.84 - .1650\sin\alpha + .0048\cos\alpha$$
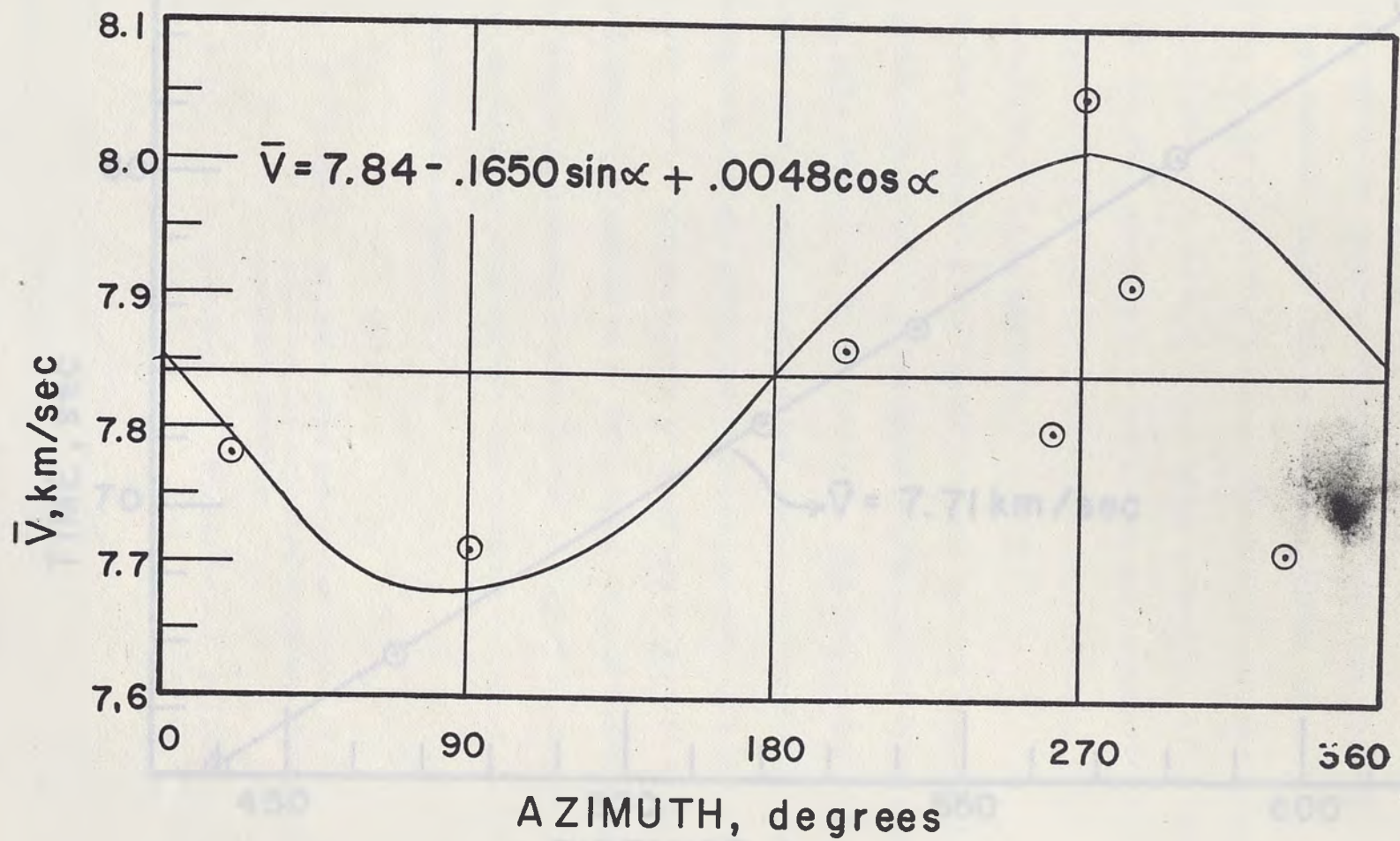
FIGURE 16. Apparent velocity vs. azimuth, REGION II.
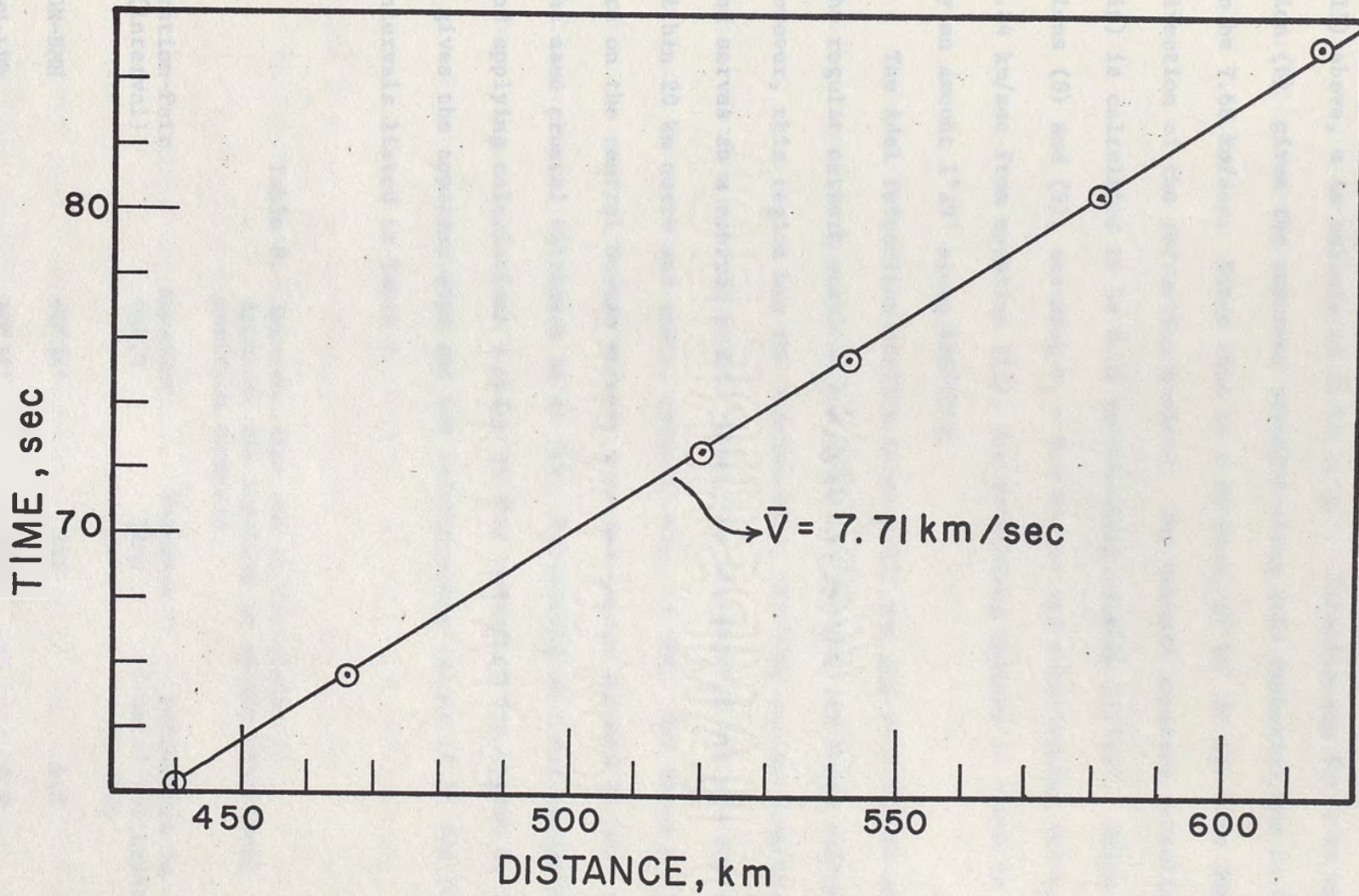
FIGURE 17. A del refraction profile.

From equation (7) and using the values of a and b from equation (13) above, α is calculated to be 91°40'. Substituting for α in equation (6) gives the apparent velocity along this direction and is found to be 7.68 km/sec. Since this is a minimum, 91°40' is the true down-dip direction of the refracting horizon. The maximum apparent velocity (up-dip) is calculated to be 8.01 km/sec along azimuth 271°40'. Using equations (8) and (9), assuming v_1 = 6.0 km/sec and substituting for v_2 = 7.84 km/sec from equation (13), the refracting horizon is found to dip by an amount 1°29' along S88°20'E.

The Adel refraction profile (Figure 17) was not recorded at any of the regular network stations and could not be used for depth calculations. However, this region has the station-pair, FPN-NRR, common with Region I and serves as a control point. Also, the stations at WON and SMN are within 20 km north and south, respectively, of FPN. All three stations are on the central Nevada seismic zone and can be assumed to have roughly the same crustal thickness as at FPN. Proceeding on these assumptions and applying calculations similar to that described for Region I, Table 8 gives the apparent dips and the corresponding values of Δh for the intervals listed in Table 7.

Table 8. Apparent dips and Δh for Region II. Apparent dip negative in up-dip direction; positive down-dip.

Station-Pair (interval)	Apparent Dip, β	Distance (km)	Difference in Crustal thickness Δh (km)
WON-BMN	+0°34'	122	1.2
BMN-LVK	+0°34'	115	0.8
WON-SMN	-0°8'	40	0.1

Based on the value of 24.5 km for the crustal thickness in the central Nevada seismic zone (Table 6), that is, for the WON-FPN-SMN area, Table 9 is representative of crustal thicknesses beneath the sites listed.

Table 9. Crustal thickness beneath sites in Region II.

Site	Crustal thickness
BMN	25.7
LVK	26.5

Region III is the eastern part of the State (Figure 11), where only 4 observations of apparent velocity were available. One is from the refraction profile extending from NTS to Boise, Idaho (Pakiser and Hill, 1963). Results from this profile were revised in 1967 (Pakiser and Hill, 1967) and the revised values have been used here. Data from nuclear explosions were made available by the U.S. Geological Survey, for their field station in Hot Creek Valley (CNPS). This station was on a line between NTS and our network station EKO, and made possible the determination of interval velocity in this region.

Figure 18 is a plot of the above four intervals on a map and Figure 19 shows the relationship between apparent velocity and azimuth.

The least-square sine curve of Figure 18 has the equation

$$\nabla = 7.75 - .1314 \sin \alpha + .2244 \cos \alpha \tag{14}$$

Substituting for $a = -.1314$, $b = .2244$, and $V_2 = 7.75$ km/sec in equations (7), (8) and (9), the refracting horizon is found to have a dip of 2°30' along direction 149°39' or S30°21'E. The calculated minimum velocity (true down-dip direction) is 7.49 km/sec and the maximum velocity (up-dip) is 8.01 km/sec.
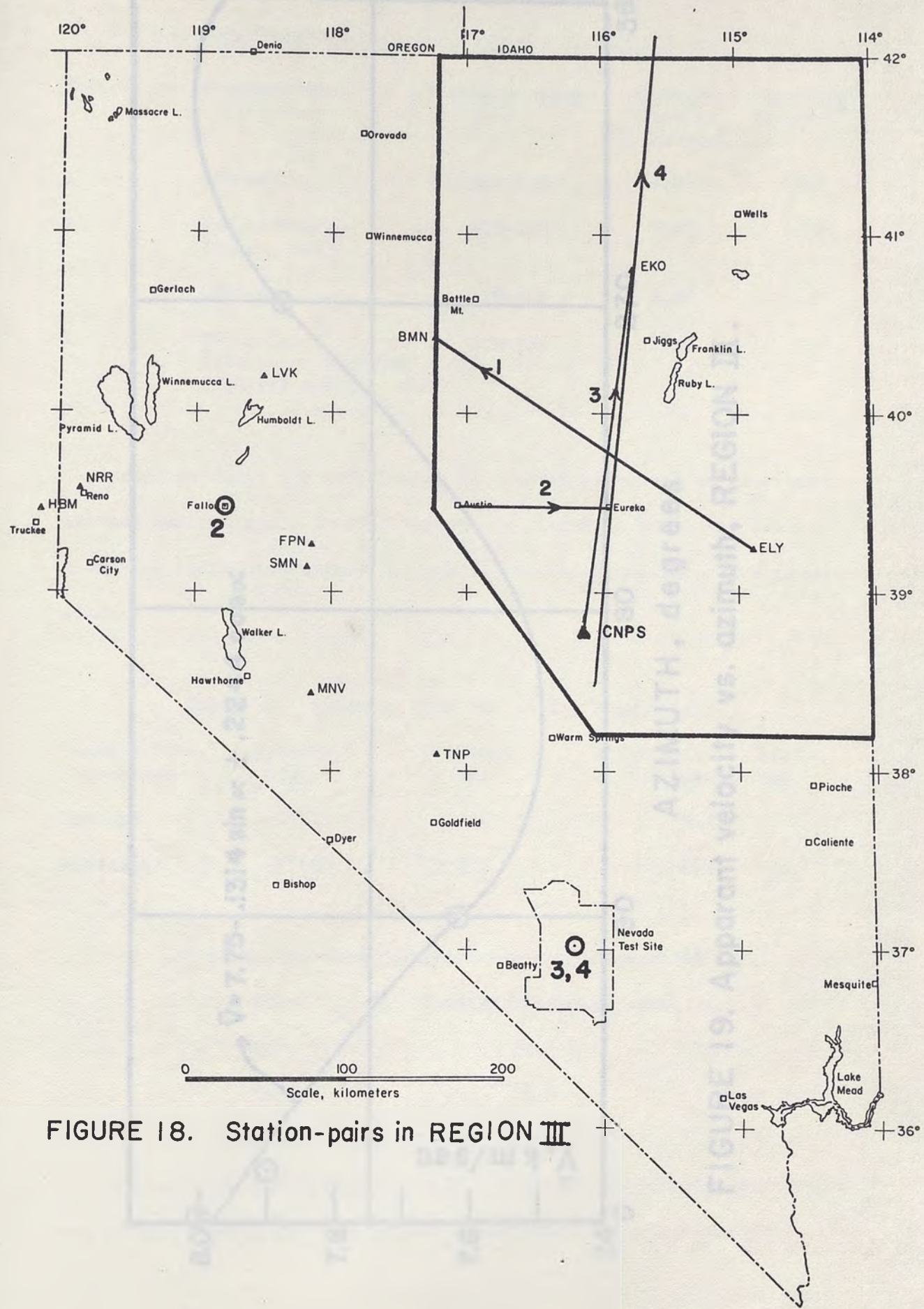
FIGURE 18. Station-pairs in REGION III
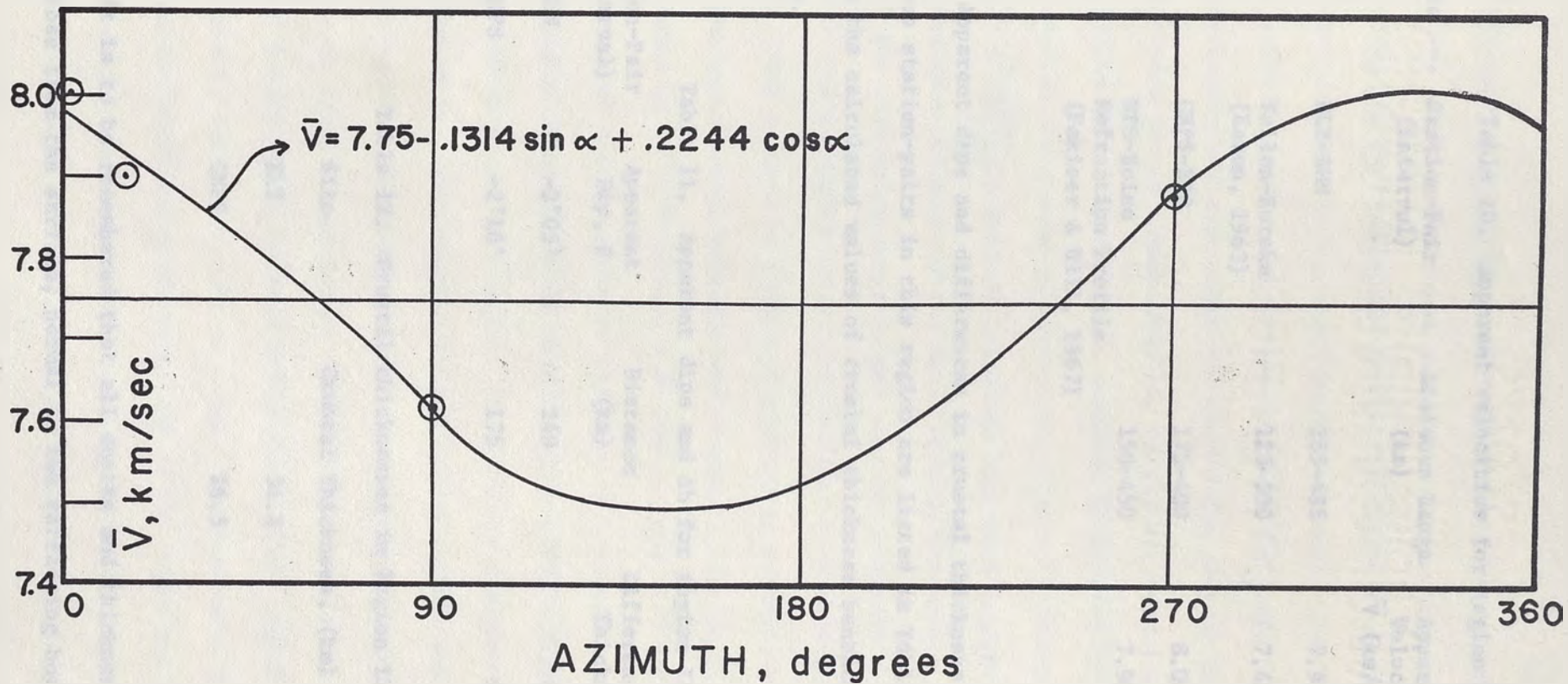
FIGURE 19. Apparant velocity vs. azimuth, REGION III.

Table 10. Apparent velocities for Region III.

Source	Station-Pair (interval)	Distance Range (km)	Apparent Velocity $\overline{V}$ (km/sec)	Azimuth (degrees)
1	ELY-BMN	255-495	7.97	300°
2	Fallon-Eureka (Eaton, 1963)	125-300	7.62	90°
3	CNPS-EKO	175-400	8.00	2°
4	NTS-Boise Refraction Profile (Pakiser & Hill, 1967)	150-450	7.90	15°

Apparent dips and differences in crustal thickness between the various station-pairs in this region are listed in Table 11; Table 12 gives the calculated values of crustal thickness beneath the various sites.

Table 11. Apparent dips and Δh for Region III.

Station-Pair (interval)	Apparent Dip, β	Distance (km)	Difference in Crustal Thickness, (km)
ELY-BMN	-2°05'	240	8.7
NTS-CNPS	-2°10'	175	6.6

Table 12. Crustal thicknesses in Region III.

Site	Crustal Thickness, (km)
ELY	34.4
CNPS	26.5

It is to be remembered that all depths and thicknesses referred to are those from the surface, normal to the refracting horizon.

Discussion and Summary. The area under investigation was divided into three regions because it was reasonable to assume that the structure would not be homogeneous across the entire State and that there would be variations in the upper mantle velocity. The division was made on an arbitrary basis, the western half of the State being divided into a northwestern and a southwestern part. The central Nevada seismic zone was included in both these regions, as several events used as sources were located here. Some common interval velocities in the two regions were used as tie points in determining crustal thicknesses, as has been shown. The eastern half of the State comprised Region III (Figure 11).

The true velocity of the upper mantle, the amount and direction of dip of the refracting horizon, and crustal thickness beneath station sites of the telemetry network, were determined separately for each region. The results of this analysis may be summarized as follows:

The upper mantle velocity for regions I, II and III (Figure 11), were found to be 7.77 km/sec, 7.84 km/sec, and 7.75 km/sec, respectively. Thus there do not appear to be large scale horizontal variations in the upper mantle velocity in the Nevada region. The average of the above three velocities is 7.79 km/sec and is to be regarded as the true P_n velocity of the upper mantle for the Nevada region, espeically the central part of the State enclosed by the telemetry network. This velocity is in excellent agreement with the P_n velocity contours for the western United States (Herrin and Taggart, 1962, and Archambeau, Flinn, and Lambert, 1969). Results of several workers under the Vela Uniform program for determining the structure of the crust and upper mantle show that the P-wave velocity in the upper mantle is around 7.7 km/sec in the southern part of the Basin and Range and tends to be nearly the

same over large areas within the province (Pakiser, 1963). Pakiser and

Hill (1967) assumed constant velocities and horizontal layers and found

a velocity of 7.90 km/sec, for their unreversed profile from NTS to

Boise, Idaho. Since the crust-mantle interface in this region (region

III in this analysis) has been shown to be dipping in a southeasterly

direction, this may be the apparent velocity along an azimuth of 15°,

roughly, and not the true velocity in the marker. The interval CNPS-EKO

along virtually the same azimuth as Pakiser and Hill's refraction profile,

shows a veloctiy of 8.0 km/sec. Ryall and Jones (1964) found a velocity

of 7.84 km/sec for the Nevada region from refraction profiles that were

widely scattered across the State and also extending into Mono Lake,

California, and Ordway, Colorado. It is not likely that the velocity

structure is homogeneous for the entire area covered by their analysis

and possibly their velocity is slightly higher than the true velocity.

Regions I and II taken together show a dip for the crust-mantle

interface of roughly 1-1/2 - 2 degrees, in a direction almost due east.

This accounts for the increase in crustal thickness from NRR (20.9 km)

to ELY (34.4 km). The structure in the eastern half of the State also

shows a predominant easterly dip (2-1/2 degrees along S30°E) and is in

accord with the overall easterly trend of the crust-mantle boundary

across the State of Nevada. This is in good agreement with the work of

Ryall and Jones (1964) who determined a broad regional dip for the

entire State and found it to be 2°12' along N84°E.

Determinations of crustal thickness beneath station sites may be

tabulated as follows:

Table 13. Crustal thicknesses across Nevada

Station	Crustal thickness (km)
NTS	33.1
NRR	20.9
TNP	29.5
MNV	28.3
FPN-SMN-WON	24.5
BMN	25.7
LVK	26.5
ELY	34.4
Fallon (Eaton, 1963)	22
Eureka (Eaton, 1963)	31-32
CNPS	26.5
EKO	31-32

These values are subject to uncertainties in the determination of
the crustal thickness beneath NTS, and in the calculations of apparent
velocities and dips. The thickness at NTS was determined from the
STINGER refraction profile (Figure 12). Differences in depth at NTS
found by various authors can be accounted for by differences in inter-
cept time, by differences in P-wave velocity both above and below the dis-
continuity, or they could be the result of some uneven configuration of
the crust-mantle interface, such as a fault, graben, or horst, beneath a
shot line. Errors in measured velocities and travel times by about two-
tenths of a second can cause variations in crustal thickness of the
order of about 1 or 2 km.

The results of this analysis indicate that the crust is increasing
in thickness eastward from NRR and thinning in a direction northward
from NTS. This would imply that the thickness at Eureka be still lower
than at CNPS. Eaton (1963) found the crustal thickness at Eureka to be
31-32 km, higher than that determined for CNPS. For the NTS-Boise re-
fraction profile, Pakiser and Hill (1967) observed unusual local delays

in P_n in the vicinity of Eureka and attributed this delay to a graben or deep depression in the M discontinuity beneath Eureka. This explains the increased crustal thickness at Eureka despite a generally thinning crust northwards from NTS. In an earlier study for the same refraction profile, Pakiser and Hill (1963) found P_n delays between Eureka and Elko (EKO), which required the crustal thickness to be increased by about 4 km between the two sites.

TIME-TERM METHOD

To determine crustal structure, the time-term method of analyzing refraction data was also employed. This has several advantages over the conventional method of interpretation, which is suitable only for a linear array of shot points and stations. The time-term approach was well-suited for the existing University of Nevada network of stations with a wide areal distribution.

The time-term interpretation in a way is a "best fit" for the crustal model, using all available data. It has often been found in previous studies that a crustal model drawn up from travel-time values for a pair of stations at one end of the network is different from a model interpreted from a pair of stations at the other end of the network. The time-term interpretation is capable of considering the relevant data from all the various shots and stations and arriving at a best fit solution to the data. The main advantages of the method are: (1) the equations can be solved without requiring the shots and stations to be laid out in any particular pattern; (2) the maximum amount of information is extracted from the data; and (3) the necessity of making simplified assumptions about the structure is minimized. The method was first suggested by Scheidegger and Willmore (1957) and improved upon by Willmore and Bancroft (1960).

The time-term method of analyzing refraction data differs somewhat from the conventional method used in refraction seismology, although not unusually so. Interpretation of all seismic refraction data assumes that the observed travel-times can be divided into groups, each of which is associated with a particular refracting horizon. In all refraction surveys, the problem is to solve unknowns in equations of the form:

$$t_{ij} = a_i + b_j + \Delta_{ij}/v \qquad (15)$$

where t_{ij} = travel time for a refracted wave beneath the shot-point and seismograph; Δ_{ij} = horizontal distance between shot-point and seismograph; a_i and b_j are "time terms" which are characteristic of the shot-point and station, repsectively; and v is the velocity of propagation of seismic waves in the underlying marker layer. The time terms associated with a particular site (shot or detector) are independent of the individual travel-time equations in which it is involved and of the time terms of neighboring sites. The time-term reflects refractor depth and local velocity variations associated with each site. These time-terms and the refractor velocity, v, are the unknowns to be determined in a set of observational equations of the type referred to as Equation (15).

It is possible to determine the values of a_i, b_j and v, which will give the "best fit" to the observed travel-times t_{ij}, if the following assumptions are made:

(1) The velocity structure beneath any site varies only with depth perpendicular to the refractor, within the cone of critically refracted rays under the site.

(2) Velocity of the base refractor is essentially constant (<∼1%), and does not have large lateral variations.

(3) The regional dip of the refractor is small (<∼5°).

(4) The curvature of the refractor is slight.

It is to be noted that the method can compensate for a curvature of the Earth and can be extended to allow for increasing velocity with depth in the marker.

Traditional methods of interpretation present considerable difficulties if the quantity of data is very large, if the velocity structure

in the region under study is complicated, and if the shots and recording stations are not aligned along a particular azimuth. Examination of the time-distance curves from a station or pair of stations are often incompatible with data from other pairs of stations. If the number of observations is considerably larger than the number of sites (including both shots and detectors), the method of least squares can be applied to minimize the sum of the squares of the residuals (observed - calculated travel-times), and hence to determine a set of time-terms and refractor velocity that best fit the theoretical travel-times to those actually observed. Given a favorable distribution of shot points and recording sites, a time-term is the result of azimuthal averaging of several observations and is representative of the closest approximation of the depth to the refracting horizon, even if the velocity structure beneath the site is complicated.

The time-term method has been successfully applied by Berry and West (1966a and b) and by Smith, Steinhart and Aldrich (1966) to determine crustal structure from explosion experiments of 1963 in Lake Superior. Hamilton (1970) also used the method in his analysis of explosion data from the vicinity of the Borrego Mountain, California, earthquake of April 9, 1968.

Smith, Steinhart and Aldrich (1966) intended the method to account for horizontal variations in the refractor velocities and also conducted model studies with constrained velocities to determine errors inherent in the assumptions of the method. Reiter (1970) conducted model experiments and computed error terms for refractor depths in case of a plane dipping refractor and a symmetrical anticlinal refractor surface.

Calculation of Time-Terms from the Observations Equations. Follow-
ing Willmore and Bancroft (1960), suppose there are n shot locations and
m recording stations, i.e., a total of (n + m) = N sites. It is then
possible, though unlikely, to obtain nxm equations of the type (15),
referred to earlier, provided all the recording sites are observing
head waves. However, the problem contains only (N + 1) unknowns, the
N time-terms associated with each shot or detector location, and the
velocity of the refracting layer.

The redundancy in the number of observations can be removed by
reducing the observational equations to a set of (n + m) normal equations.
The normal equation referring to the ith shot can be put in the form

$$m_i(a_i - \alpha) = \sum_{j+1}^{m} (t_{ij} - \Delta_{ij}/v) - \sum_{j+1}^{m} (b_j + \alpha) \tag{16}$$

This is obtained by adding together all the observational equations which
contain observations from a given station, or of a given shot.

m_i is the number of stations which observed the ith shot and, α is
an arbitrary constant which is subtracted from all the shot terms, a_i,
and added to all the station terms, b_j, thereby leaving the observational
equations unaltered. This shows that all the unknowns cannot be deter-
mined uniquely, and hence the solution will be subject to the ambiguity
existing in the arbitrary constant α. It will be shown later how this
uncertainty in the solution can be overcome.

The normal equation for the jth station can, similarly, be written

$$n_j(b_j + \alpha) = \sum_{i+1}^{n} (t_{ij} - \Delta_{ij}/v) - \sum_{i+1}^{n} (a_i - \alpha) \tag{17}$$

n_j is the number of shots recorded by the station.

If all the stations observe all the shots, $m_i = m$ and $n_j = n$.

Eliminating b_j between (16) and (17) we have

$$(a_i - \alpha) = \frac{1}{m}\sum_{j=1}^{m}(t_{ij} - \Delta_{ij}/v) - \frac{1}{nm}\sum_{j=1}^{m}\sum_{i=1}^{n}(t_{ij} - \Delta_{ij}/v) + \frac{1}{n}\sum_{i=1}^{n}(a_i - \alpha) \quad (18)$$

Since the last term on the right hand side of equation (18) already contains an ambiguity, we can assume one time-term arbitrarily, in such a way as to reduce $\sum_{i=1}^{n}(a_i - \alpha)$ to zero.

Then equation (18) becomes:

$$a_i = \frac{1}{m}\sum_{j-1}^{m}(t_{ij} - \Delta_{ij}/v) - \frac{1}{nm}\sum_{j=1}^{m}\sum_{i=1}^{n}(t_{ij} - \Delta_{ij}/v) + \alpha \quad (19)$$

and, solving for b_j from equation (17),

$$b_j = \frac{1}{n}\sum_{i=1}^{n}(t_{ij} - \Delta_{ij}/v) - \alpha \quad (20)$$

Substituting for the time-term a_i and b_j into the observational equations, we obtain nm equations of the form

$$\frac{1}{m}\sum_{j=1}^{m}(t_{ij} - \Delta_{ij}/v) - \frac{1}{nm}\sum_{j=1}^{m}\sum_{i=1}^{n}(t_{ij} - \Delta_{ij}/v) + \frac{1}{n}\sum_{i=1}^{n}(t_{ij} - \Delta_{ij}/v) =$$

$$t_{ij} - \Delta_{ij}/v - R_{ij} \quad (21)$$

R_{ij} is the residual of the observation = (observed - calculated) travel-time.

Equation (21) can be rewritten in the form

$$c_{ij} - \frac{1}{v}d_{ij} = R_{ij} \quad (22)$$

where $c_{ij} = -\frac{1}{m}\sum_{j=1}^{m}t_{ij} + \frac{1}{nm}\sum_{i=1}^{n}\sum_{j=1}^{m}t_{ij} - \frac{1}{n}\sum_{i=1}^{n}t_{ij} + t_{ij}$ \quad (22a)

and, $d_{ij} = -\frac{1}{m}\sum_{j=1}^{m}\Delta_{ij} + \frac{1}{nm}\sum_{i=1}^{n}\sum_{j=1}^{m}\Delta_{ij} - \frac{1}{n}\sum_{i=1}^{n}\Delta_{ij} + \Delta_{ij}$ \quad (22b)

Using a least squares approximation, the best value for v is

$$\frac{1}{v} = \frac{\sum c_{ij}\, d_{ij}}{\sum d^2_{ij}} \qquad (23)$$

Substituting for v in Equation (19) and (20), we obtain all values of a_i and b_j, subject to the ambiguity contained in the arbitrary constant α.

To determine α, some shot points and recording sites can be put at the same location. This will give several values of d_{ij} for which $a_i = b_j$, in equations (19) and (20). The mean value of α_{ij} determined from all available values is then considered to be the best estimate for α. If this procedure cannot be followed for a particular survey, α can be estimated from the known geology.

So far, only the case when all the stations observe all the shots has been considered. To account for the possibility of missing observations, let us define a quantity γ_{ij} so that $\gamma_{ij} = 1$, when T_{ij} exists as data and $= 0$, when it does not exist.

$$T_{ij} = \text{observed travel-time}$$

$$= t_{ij} + R_{ij}$$

So that

$$R_{ij} = T_{ij} - t_{ij}$$

$$= T_{ij} - \frac{\Delta_{ij}}{v} - a_i - b_j$$

or, $R_{ij} = X_{ij} - a_i - b_j$ $\qquad (24)$

where,

$$X_{ij} = T_{ij} - \frac{\Delta_{ij}}{v} \qquad (25)$$

The sum of the squares of the residuals, I, can be written

$$I = \sum_{i=1}^{N} \sum_{j=1}^{N} [X_{ij} - a_i - b_j]^2 \gamma_{ij}$$

$$= \sum_{i=1}^{N} \sum_{j=1}^{N} X^2_{ij}\gamma_{ij} + a^2_i \sum_{j=1}^{N} \gamma_{ij} + \sum_{j=1}^{N} a^2_j\gamma_{ij} - 2a_i \sum_{j=1}^{N} X_{ij}\gamma_{ij}$$

$$-2 \sum_{j=1}^{N} a_j X_{ij}\gamma_{ij} + 2a_i \sum_{j=1}^{N} a_j\gamma_{ij} \tag{26}$$

Minimizing I with respect to each time-term, we have the condition:

$$\frac{\delta I}{\delta a_i} = 0 = 0 + 2a_i \sum_{j=1}^{N} \gamma_{ij} + 0 - 2\sum_{j=1}^{N} X_{ij}\gamma_{ij} - 0 + 2\sum_{j=1}^{N} a_j\gamma_{ij}$$

or, $$\sum_{j=1}^{N} X_{ij}\gamma_{ij} = a_i\sum_{j=1}^{N} \gamma_{ij} + \sum_{j=1}^{N} a_j\gamma_{ij} \tag{27}$$

The ith equation of the set of N linear simultaneous equations can be written,

$$\sum_{j=1}^{N} X_{ij}\gamma_{ij} = a_i\sum_{j=1}^{N} \gamma_{ij} + \sum_{j-1}^{i-1} a_j\gamma_{ij} + \sum_{j=1}^{N} a_j\gamma_{ij} \tag{28}$$

In matrix notation

$$[c_{ij}] [a_j] = [\bar{x}_i] \tag{29}$$

or, $C \times A = \bar{X}$ $\tag{30}$

where,

$$
\left.
\begin{array}{l}
c_{ij} = \gamma_{ij}, \; i \neq j \\[2mm]
c_{ii} = \sum_{j=1}^{N} \gamma_{ij} \\[2mm]
\bar{x}_i = \sum_{j=1}^{N} X_{ij}\gamma_{ij}
\end{array}
\right) \tag{31}
$$

Equation (30) is solved by inverting C, the coefficient matrix,
multiplying it by X, the data matrix, to yield the time-term

matrix A, or, $A = C^{-1} \times \overline{X}.$ (32)

The fit of a time-term model (Berry and West, 1966a and b) to the observational data is given by the standard deviation of the solution

$$\sigma^2 = \frac{\sum\limits_{j=1}^{N} \sum\limits_{i=1}^{N} R_j^2 \gamma_{ij}}{\sum\limits_{j=1}^{N} \sum\limits_{i=1}^{N} \gamma_{ij} - N}$$ (33)

Drawbacks of a time-term survey

Since the calculation of the time-term depends on the refractor velocity, v, it is important to have effective controls in determining v. The residuals R_{ij} represent the inconsistencies of the observations and all the uncertainties in v are reflected in the values of R_{ij}. The standard deviation $\sigma\left(\frac{1}{v}\right)$ in $\frac{1}{v}$ can be written

$$\sigma^2\left(\frac{1}{v}\right) = \frac{\sigma^2(t)}{\sum d_{ij}^2}$$ (34)

From equation (22b),

$$d_{ij} = \Delta_{ij} - \frac{1}{m}\sum_{j=1}^{m} \Delta_{ij} - \frac{1}{n}\sum_{i=1}^{n} \Delta_{ij} + \frac{1}{nm} \sum_{i=1}^{n} \sum_{j=1}^{m} \Delta_{ij}$$ (35)

If all the stations are close together, the first two terms on the right-hand side of equation (35) will almost cancel. If all the shots are close together, the first and third terms will almost cancel. Hence for an accurate determination of the velocity, both shots and recording locations should have a wide areal distribution. This deduction is based on the assumption that each new observation reduces the uncertainty in $\frac{1}{v}$ by its contribution to $\sum d_{ij}^2$ in equation (34). This is largely

true since $\sigma^2(t)$ tends to a constant value if the number of available observations of given quality is very large.

Errors in the time-term values can be introduced by local velocity variations in the marker layer, which affect all travel-time values of a particular shot or receiver. The time-term method is not capable of detecting those errors since the method is based on the assumption that there are no horizontal variations of velocity in the marker layer. Errors of this type are especially likely for sites at the fringes of the network, for ray paths through the marker to and from such sites, may not coincide with ray paths through the marker for other points of the network.

The time-term method also requires that the observed first arrivals be head waves of the lateral wave type. The method breaks down if the observed waves are continuously refracted from deeper layers with in-creasing shot-station distance. However, this is easy to detect for in the event of continuously refracted waves, the travel-time curves would show a systematic trend toward higher apparent velocities with increasing shot-station distances. A plot of residuals against shot-station distance would show an early-late-early trend. If the residuals are negative at the shortest and longest distances, this shows that velocity in the marker is increasing with depth. If two residuals have the same sign but different magnitudes, and associated with ray paths of different length but all passing through the same area of the ground, this suggests a lateral variation of velocity of limited horizontal extent (Willmore and Bancroft, 1960).

To further confirm the hypothesis that the observed waves are head waves, a plot can be made of the standard deviation of a solution against

the assigned refractor velocity. If the standard deviation shows a distinct minimum with respect to a refractor velocity, it has been demonstrated that the basic assumptions of the method have been reasonably fulfilled.

Difficulties Encountered in the Time-Term Analysis. The time-term approach for determining crustal structure and velocity was intended to corroborate the results of the analysis already described. It was thought that with the existing University of Nevada telemetry network with a wide areal distribution of stations, and nuclear explosions in the southern part of the State (NTS), to serve as seismic sources, along with mine blasts at Ely, Battle Mountain, Gabbs, and Yerington, this would be an ideal situation to implement the time-term method. But several difficulties became evident:

(i) The mine blasts were generally not large enough to record the P_n phase at most or even some of the network stations, except at those which were close enough to the mining operation. An analysis of this type requires several events to be recorded at most of the sites. Only one blast at Ely proved large enough to record P_n at most of the network stations.

(ii) Earthquakes located within the network could not be used as sources because they had varying depths and upset the time-term values in an unpredictable way, if combined with nuclear explosions and mine blasts. Besides, there were not sufficient earthquakes recording the P_n phase at most of the stations. There were perhaps 10 such events between Oct., 1969, through June, 1970, which recorded consistently at 4 of the stations; most earthquakes recorded P_n at only 2 or sometimes 3 stations. Since P_g recorded very prominently

on all our stations consistently, it was thought possible to use
P_g for a time-term solution for an upper refractor, the interface
between the sedimentary layer and the earth's crust. But the foci
of the events were invariably below this interface and led to
highly erroneous calculations of time-terms from the observational
equations. However, earthquakes proved useful in determining both
P_n and P_g velocities, because of the azimuthal averaging that re-
sulted from the random distribution of events about the network
stations.

(iii) The only events which could be used as sources then, for
waves refracted from the Mohorovicic discontinuity, were nuclear
explosions from NTS. Although the recording sites had a fairly
wide areal distribution, the shot points were clustered together,
thereby introducing large errors in velocity determination. From
equation (34), the standard deviation
$\sigma^2\left(\frac{1}{v}\right)$ of a particular computed velocity is

$$\sigma^2\left(\frac{1}{v}\right) = \frac{\sigma^2(t)}{\sum d^2_{ij}} \tag{34}$$

where

$\sigma(t)$ is the standard deviation of a time term and d_{ij} is a function
of the distances between shot points and stations. From equation (35)
it can be seen that if shot points and/or stations become
clustered together, d_{ij} tends to zero and $\sigma\left(\frac{1}{v}\right)$ tends to infinity
(Willmore and Bancroft, 1960). Besides, as has been shown, the M
discontinuity in Nevada is dipping in a southeasterly direction and
hence all refracted waves from NTS travelling northwestwards

essentially to the recording stations, propagate along the up-dip direction. Reiter (1970) has shown from model experiments that unless shot points are located both up-dip and down-dip from stations, this could lead to unrealistic velocity determinations.

(iv) The angle of dip of the ray path is a crucial factor in determining error magnitudes and Reiter found that in the case of either a dipping plane refractor or a symmetric anticline, the sum of the computed refractor depths beneath a shot point and a station would be less than the sum of the true depths. Reiter (1970) also discovered that the best reconstruction of the structure is achieved not at the true velocity but at a slightly higher velocity. It is not certain how much the results of this analysis have been affected by Reiter's hypotheses. From interval velocities, it appears that the structure in Nevada is fairly homogeneous although local anomalies in the crustal structure may exist, as is evident from station delays at some sites, already discussed.

(v) The time-term method assumes that the refractor velocity should not have large scale velocity variations and, perhaps should be less than 1 percent (Berry and West, 1966). The interval-velocity analysis has shown that variations from 1-2 percent (7.75-7.84) km/sec are probably present in Nevada, although this would not, perhaps, affect the results too seriously. Dips too, as revealed by the previous analysis, are within allowable limits.

(vi) Difficulty was encountered in determining the constant term, α, which controls the uniqueness of the solution. Since this was not a conventional survey, it was not possible to have some common shot points and seismograph locations. α was set equal to 3.5 sec

based on the crustal thickness calculated for NTS from the analysis
already described.

Analysis and Results. A computer program (Appendix I) utilizing
travel-times and distances from the located event to the recording sites
was developed, which calculates a least-squared velocity from all avail-
able observations, determines the time terms for each site (shot point or
station), converts the time terms into their corresponding depths, and
calculates the residual (observed-calculated travel-time) of each observation.
The program also computes time-term solutions at various constrained velo-
cities and determines the standard deviation of each solution. For these
calculations, the observations used were those in which all the events
were observed by all stations of the network, or, at least by the same
stations of the network, for a particular experiment. Appropriate weight
was given to the computations when this was not possible.

The experimental data, both travel-times and distances for the
observed P_n phase from located earthquakes, all of which recorded at
the 4 stations, NRR, TNP, LVK and BMN, are given in Table 14, along with
the residual determined for each observation. A run with this data
gave a P_n velocity close to 7.5 km/sec, with a standard deviation of
1.2 sec. The large standard deviation is due to the somewhat large
residuals, especially for observations from events which were located
outside the network. The true velocity determined from interval velo-
cities earlier is 7.79 km/sec and this discrepancy is probably due to
mislocation of some events used in this run or perhaps due to observa-
tions of poor quality. In another experiment using 14 nuclear explosions
and 6 stations, it was noted that an error of 2 sec in 1 observation out
of 84, changed the velocity determined by as much as 0.33 km/sec.

Table 14. Travel-times, distances, and P_n residuals from 10 Nevada earthquakes.

Event	Dist.	NRR T.T.	Res.	Dist.	TNP T.T.	Res.	Dist.	LVK T.T.	Res.	Dist.	BMN T.T.	Res.
1	348.8	49.7	-.331	355.4	51.8	1.822	452.3	62.4	-.720	532.6	72.7	-.771
2	160.7	26.2	-.203	132.1	21.6	- .046	130.7	21.4	-.247	169.9	27.0	.496
3	410.0	56.6	-1.202	130.0	20.3	.862	381.5	53.3	.054	358.7	50.1	.285
4	163.5	26.7	-.814	127.9	22.5	.680	135.2	22.7	-.285	173.2	28.1	.419
5	124.8	21.6	-.094	189.5	31.0	1.592	198.6	30.4	-.413	279.8	40.2	-1.084
6	307.0	45.0	-.381	117.6	18.2	-.928	232.3	35.3	.651	183.5	28.4	.657
7	300.6	48.0	2.005	116.9	17.9	-2.604	225.6	36.3	1.077	178.0	28.0	-.477
8	160.5	27.0	.231	135.5	23.0	.508	126.3	20.9	-.551	164.6	26.0	-.188
9	190.5	31.2	1.746	93.2	13.2	-2.313	199.0	30.2	.356	239.6	35.1	.212
10	663.1	89.2	-.957	418.1	56.9	.428	576.4	77.9	.078	487.7	66.3	.451

Apparently then to calculate the velocity from equation (9), all observations need to be of excellent quality; a single large residual could produce a highly erroneous result.

Time-terms and their corresponding depths could not be calculated to any degree of certainty, because α could not be determined. Besides, earthquakes with varying depths alter the observational equations from which time-terms are calculated, in an unpredictable way; unless the depth of focus of each event is known, from which correction terms can be calculated.

An analysis employing 102 observations from 17 nuclear explosions at NTS, all of which were recorded by 6 stations of the network (JAS, NRR, LVK, BMN, TNP, and ELY) gave a P_n velocity of 7.7 km/sec. However, other experiments varying the number of shots and recording sites used gave velocities ranging from 6.7 km/sec to 7.9 km/sec, for P_n. Since velocity determinations were so unreliable, presumably because of observations of poor quality (although care was taken to avoid these), and more so due to lack of azimuthal averaging from not having shots and stations distributed randomly, constrained velocity solutions were generated for each set of data, for velocities ranging from 7.0 km/sec to 8.5 km/sec. A solution at each constrained velocity, calculated the standard deviation of the solution, the time-terms and depths associated with sites included and the residual of each observation involved. It was found using different sets of data (changing the number of shots and stations involved), that although the true velocity determined by the program varied, time-terms and depths calculated at a particular constrained velocity were fairly consistent for a particular site (shot or station).

| EVENT	JAS			NRR			LVK			BMN			TNP			ELY			EUR			MNV			CNPS		
	Dist.	T.T.	Res.	Dist.	T.T.	Res.	Dist.	T.T.	Res.	Dist.	T.T.	Res.	Dist.	T.T.	Res.	Dist.	T.T.	Res.	Dist.	T.T.	Res.	Dist.	T.T.	Res.	Dist.	T.T.	Res.
GRAPE B	394.8	57.6	.180	429.6	61.5	-.636	405.7	57.5	-.261	384.8	55.1	.103	151.0	25.8	.220	254.8	38.9	.100	264.9	40.2	.072	238.9	36.9	.184	185.8	30.2	.038
LABIS	391.9	57.1	.015	424.1	61.5	.033	398.9	56.7	-.226	377.5	54.4	.303	145.0	24.7	-.146	248.5	38.0	-.028	257.6	39.1	-.128	233.5	36.2	.140	178.5	29.3	.038
DIANA MIST	376.8	55.3	.017	410.3	60.0	.169	387.7	55.3	-.324	369.7	53.4	.168	131.9	23.0	-.301	250.7	38.5	.053	254.2	39.0	.072	219.3	34.4	.027	173.7	28.9	.118
CUMARIN	398.8	58.0	.006	435.9	62.2	-.805	412.7	58.7	-.021	392.1	55.9	-.095	157.6	26.8	.312	260.3	39.5	-.067	271.6	41.3	.251	245.0	37.7	.140	192.8	31.4	.279
YANNIGAN	390.9	57.3	.116	425.7	61.4	-.499	402.1	57.9	.336	381.9	55.1	.211	147.1	25.3	-.043	254.3	39.1	.100	262.9	39.8	-.336	234.8	36.6	.146	183.5	30.1	-.031
CYATHUS	387.2	55.7	-.150	419.9	60.1	-.197	395.5	55.5	-.358	375.3	53.1	-.084	141.0	23.4	-.302	249.3	37.7	.200	256.7	38.8	.319	229.2	34.7	-.177	177.1	29.2	.749
ARABIS	393.0	57.5	-.070	426.2	62.0	-.080	401.4	58.0	.410	380.3	54.6	-.188	147.2	25.3	-.173	250.8	38.6	-.067	260.3	40.5	.582	235.5	36.4	-.261	181.2	29.8	-.152
JAL	397.9	58.3	-.063	436.9	63.5	-.118	415.0	59.8	.300	395.3	56.6	-.290	159.3	27.4	.210	264.7	40.5	-.116	275.6	42.3	.254	246.1	38.2	.015	196.6	31.9	-.193
SHAFER	395.5	57.8	.112	430.9	62.0	-.480	407.0	57.8	-.306	386.2	55.4	.045	152.3	26.2	.276	255.9	39.2	.081	266.2	40.8	.327	240.1	37.0	-.048	187.1	30.5	-.097
SNUBBER	399.2	58.2	.084	435.3	62.9	-.099	411.5	58.6	-.037	390.4	55.7	-.147	156.8	26.7	.245	258.1	39.4	.045	269.6	40.9	.037	244.6	37.6	.021	190.9	30.8	-.148
BEEBALM	395.0	57.6	-.212	426.6	62.1	-.017	402.0	58.1	.448	380.9	54.8	-.063	147.7	25.5	-.022	251.5	38.6	-.142	261.0	40.2	.207	235.9	36.7	.003	181.7	29.8	-.201
HOD	395.7	57.8	-.044	432.3	62.7	-.091	409.3	58.9	.368	389.0	55.7	-.145	154.1	26.5	.214	258.9	39.4	-.235	269.2	41.2	.212	241.5	37.3	-.058	190.1	30.8	-.222
MINT LEAF	378.3	55.6	.073	410.6	59.7	-.222	387.2	55.6	-.012	368.5	53.4	.270	131.9	23.1	-.253	248.4	38.4	.196	252.4	38.7	-.048	219.8	34.6	.110	172.0	28.5	-.115
CORNICE	392.0	57.5	-.064	424.3	65.0	3.041	399.1	57.1	-.317	377.7	54.5	-.089	145.2	25.1	-.238	248.7	38.4	-.120	257.8	37.9	-1.820	233.6	36.3	-.239	178.7	29.6	-.154
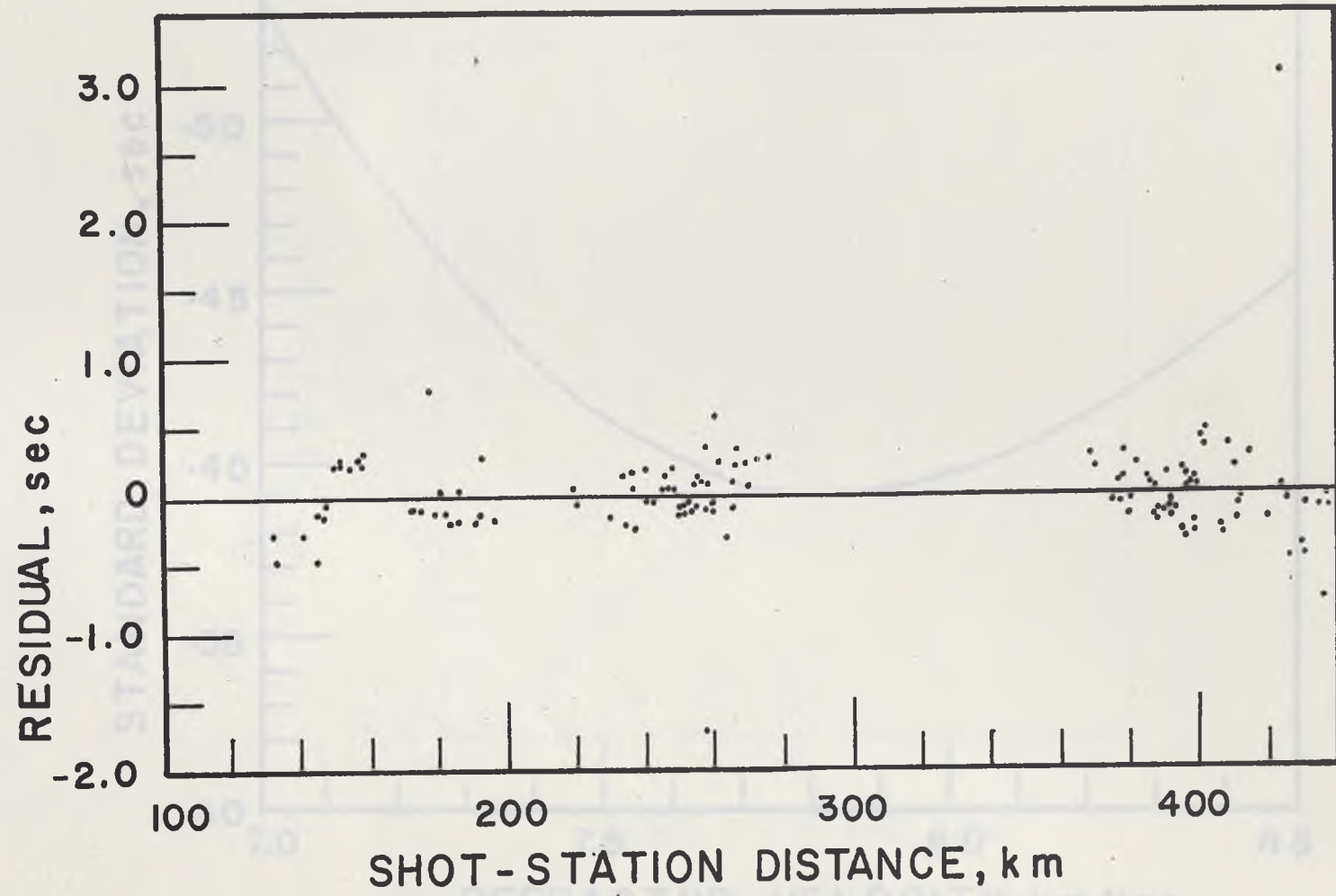
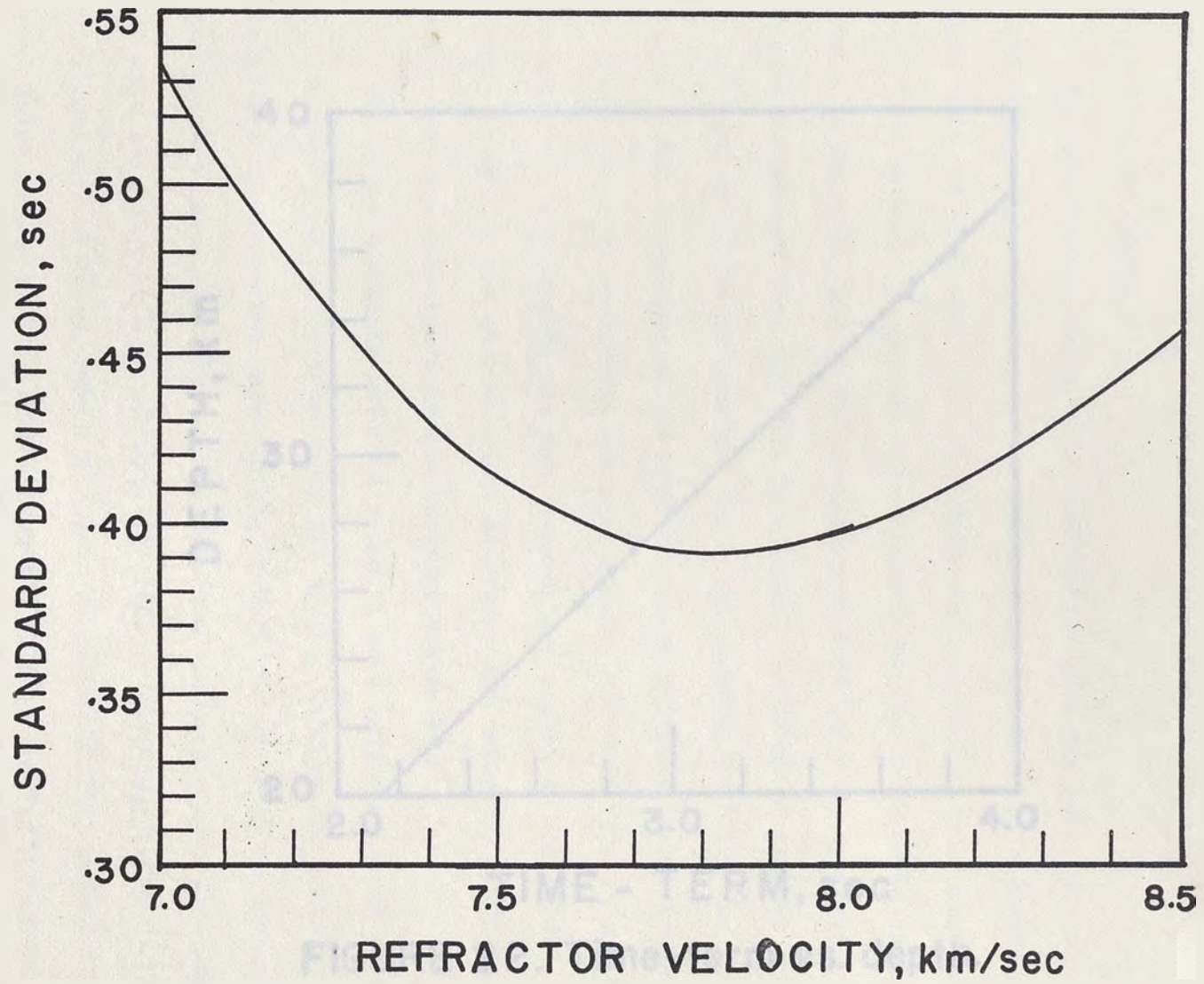FIGURE 20. Residual vs. shot-station distance.

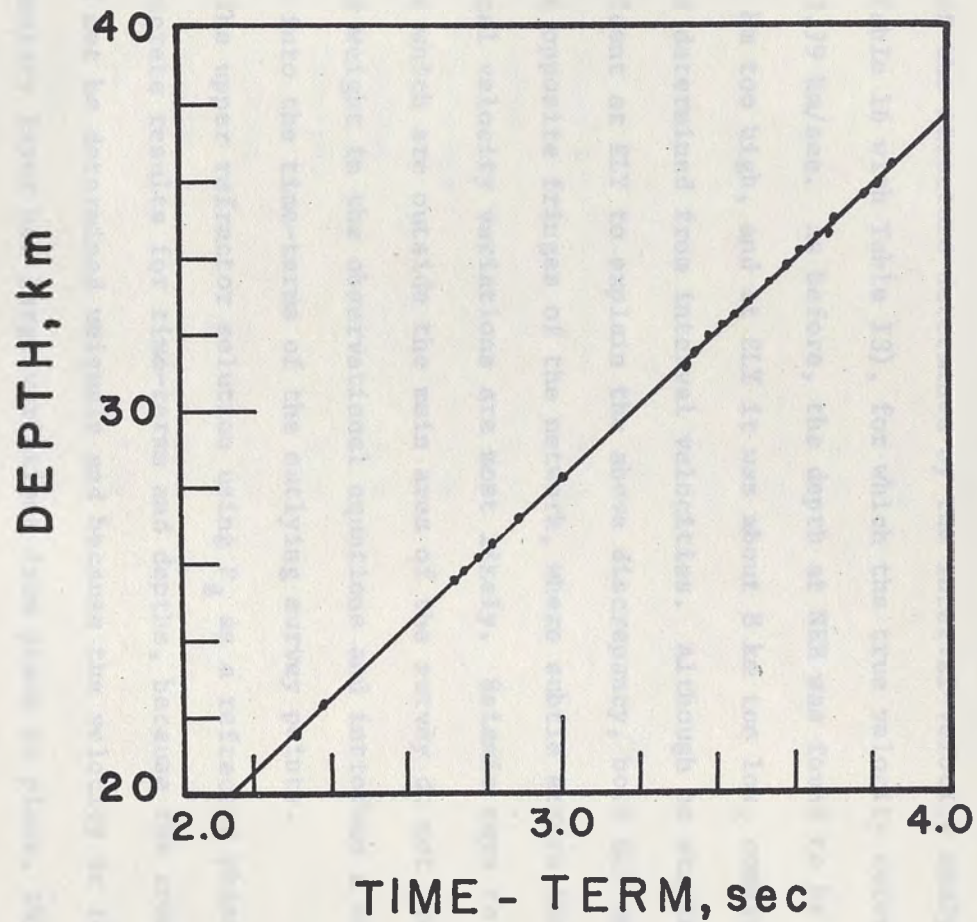FIGURE 21. Std. deviation vs. refractor velocity.

FIGURE 22. Time-term vs. depth.

velocity shows a distinct minimum at 7.8 km/sec, the best fitting velo-
city, and confirms the above observation. Table 16 shows the time-
terms, and corresponding depths for the various sites at a constrained
velocity of 7.79 km/sec, and Figure 22 shows the relationship between
time-term and depth.

The constrained velocity of 7.79 km/sec gave the best representa-
tion of the structure determined by the interval-velocity analysis (com-
pare Table 16 with Table 13), for which the true velocity determined was
also 7.79 km/sec. As before, the depth at NRR was found to be about
10-12 km too high, and at ELY it was about 8 km too low, compared to the
depths determined from interval velocities. Although no station delay
is evident at ELY to explain the above discrepancy, both ELY and NRR
are at opposite fringes of the network, where subtle errors introduced
by local velocity variations are most likely. Seismic rays to and from
points which are outside the main area of the survey do not receive
proper weight in the observational equations and introduce a concealed
error into the time-terms of the outlying survey points.

The upper refractor solution using P_g as a refracted phase produced
no concrete results for time-terms and depths, because the constant α
could not be determined uniquely and because the velocity in the upper
sedimentary layer has large variations from place to place, thus making
it hard to assign it a fixed value in order to make meaningful
computations. However, owing to a good dispersal of shot points in this
case (mine blasts at Ely, Battle Mountain, Gabbs, and Yerington and
nuclear explosions at NTS), calculations of the refractor velocity gave
good results and was found to be 6.0 $\pm$ 0.05 km/sec for various sets of
data.

Table 16. Time-terms and corresponding depths at 7.79 km/sec, $\alpha = 3.5$, $v_1 = 6.0$ km/sec.

Site	Time-Term (sec)	Depth (km)
JAS	3.42	32.2
NRR	3.67	34.5
LVK	2.37	22.3
BMN	2.29	21.5
TNP	2.88	27.1
ELY	2.78	26.1
EUR	2.81	26.4
MNV	2.73	25.7
CNPS	3.0	28.2
Nuclear Grape B	3.32	31.2
" Labis	3.35	31.5
" Diana Mist	3.49	32.8
" Cumarin	3.38	31.8
" Yannigan	3.58	33.7
" Cyathus	2.72	25.6
" Arabis	3.70	34.8
" Jal	3.86	36.3
" Shaper	3.49	32.9
" Snubber	3.45	32.4
" Beebalm	3.68	34.6
" Hod	3.62	34.1
" Mint Leaf	3.54	33.3
" Cornice	3.82	35.9

Conclusions.

1.   A good determination of the refractor velocity is not possible unless all observations are of high quality; a single large residual could affect the velocity calculation considerably.

2.   Wide dispersal of shot points and stations are absolutely essential for accurate velocity determinations.

3.   Time-terms, and consequently depths, associated with a particular site can be offset considerably if station delays are present owing to local complications in the structure beneath the site.

4.   Time-terms and depths determined at the fringes of the network are highly unreliable.

5.   Shots or events used as sources should all be of the same depth approximately; sources with varying depths cause unpredictable errors in time-term calculations. Naturally-occurring earthquakes should be avoided for this type of analysis. Depth of the source should not be below the refractor.

SUGGESTIONS FOR FURTHER WORK

For a proper implementation of the time-term method it has been
shown that a wide dispersal of shots and stations is highly desirable.
Mine blasts of the magnitude of that detonated at Ely, Nevada, on
June 6, 1970, could also be detonated at other sites of mining opera-
tions across the State, namely at Gabbs, Yerington and Battle Mountain.
This would improve greatly the results of the time-term analysis. If
advance notice of the date of explosion of these large shots can be
obtained, it would be possible to arrange for some common seismographic
locations and shot points, such as at Ely and Battle Mountain. This
would permit the direct determination of the constant term α, which
was assigned a value based on other considerations in this study. For
a more accurate determination of time-terms corrections for inclined
ray paths could be made. Willmore and Bancroft (1960) determined
correction terms for various values of v_1/v_2 and angles of incidence.

To confirm the determinations of P_n velocity, reversed refraction
profiles would obviously be most appropriate. Such refraction work
should be carried out at places where the structure is somewhat in doubt
or complicated, such as under the FPN-SMN area, between LVK and BMN and
at the fringes of the Sierra Nevada mountain ranges, that is, in the
NRR-HBM-JAS area.

REFERENCES

Archambeau, C.B., E. A. Flinn, and D. G. Lambert, 1969, Fine structure of the upper mantle, Jour. Geophys. Res., vol. 74, no. 25, p. 5825.

Berry, M.J., and G. F. West, 1966a, An interpretation of the first-arrival data of the Lake Superior experiment by the time-term method, Bull. Seism. Soc. Am., vol. 56, p. 141.

Berry, M.J., and G. F. West, 1966b, A time-term interpretation of the first-arrival data of the 1963 Lake Superior experiment, Am. Geophys. Union, Geophys. Monograph 10, p. 166.

Eaton, J.P., 1963, Crustal structure from San Francisco, California, to Eureka, Nevada, from seismic refraction measurements, Jour. Geophys. Res., vol. 68, no. 20, p. 5789.

_____, 1966, Crustal structure in northern and central California from seismic evidence, Geology of Northern California, Calif. Div. Mines and Geol. Bull. 190, p. 419.

Hamilton, R.M., 1970, Time-term analysis of explosion data from the vicinity of the Borrego Mountain, California, earthquake of 9 April, 1968, Bull. Seism. Soc. Am., vol. 60, no. 9, p. 367.

Herrin, E. and J. Taggart, 1962, Regional variations in P_n velocity and their effect on the location of epicenters, Bull. Seism. Soc. Am., vol. 52, p. 1037.

Hill, D.P., 1963, Gravity and crustal structure in the western Snake River Plain, Idaho, Jour. Geophys. Res., vol. 68, no. 20, p. 5807.

Hill, D.P., and L. C. Pakiser, 1963, Crustal structure from seismic refraction measurements between Eureka, Nevada, and Boise, Idaho, Trans. Am. Geophys. Union, vol. 44, p. 890.

Knopoff, L. and T. L. Teng, 1965, Analytical calculation of the seismic travel-time problem, Reviews of Geophys., vol. 3, p. 11.

O'Brien, P.N.S., 1968, Lake Superior crustal structure - A reinterpretation of the 1963 seismic experiment, Jour. Geophys. Res., vol. 73, no. 8, p. 2669.

Pakiser, L.C., 1963, Structure of the crust and upper mantle, western United States, Jour. Geophys. Res., vol. 68, no. 20, p. 5747.

Pakiser, L.C., and D. P. Hill, 1963, Crustal structure in Nevada and southern Idaho from nuclear explosions, Jour. Geophys. Res., vol. 68, no. 20, p. 5757.

Pakiser, L.C., and D. P. Hill, 1967, Seismic refraction study of crustal structure between the Nevada Test Site and Boise, Idaho, Geol. Soc. Am. Bull., vol. 78, p. 685.

Pakiser, L.C., W. H. Jackson, S. W. Stewart, D. J. Stuart, J. H. Healy,
    J.F. Cooper, J. P. Eaton, C.B. Forbes, C.J.Frankovitch and J.C.
    Roller, 1962, Crustal structure in the western United States,
    Report prepared by U.S. Geological Survey, Dept. of the Interior
    for the VELA UNIFORM program, Advanced Research Projects Agency,
    Department of Defense.

Press, Frank, 1960, Crustal structure in the California-Nevada region,
    Jour. Geophys. Res., vol. 65, p. 1809.

Reiter, L., 1970, An investigation into the time-term method in Refrac-
    tion Seismology, Bull. Seis. Soc. Am., vol. 60, p. 1.

Roller, J.C., and J. H. Healy, 1963, Crustal structure between Lake Mead,
    Nevada, and Santa Monica Bay, California, from seismic refraction
    measurements, Jour. Geophys. Res., vol. 68, no. 20, p. 5837.

Ryall, Alan, 1962, The Hebgen Lake, Montana, earthquake of August 18,
    1959; P waves, Bull. Seism. Soc. Am., vol. 52, p. 235.

Ryall, Alan and A. E. Jones, 1964, Computer programs for automatic pro-
    cessing of Basin and Range seismic data, Bull. Seis. Soc. Am.,
    vol. 54, no. 6, p. 2295.

Ryall, Alan and D.J. Stuart, 1963, Travel-times and amplitudes from
    nuclear explosions: Nevada test site to Ordway, Colorado, Jour.
    Geophys. Res., vol. 68, no. 20, p. 5821.

Ryall, Alan, J.D. Van Wormer, and A. E. Jones, 1968, Triggering of
    microearthquakes by earth tides, and other features of the Truckee,
    California, earthquake sequence of September, 1966, Bull. Seis. Soc.
    Am., vol. 58, no. 1, p. 215.

Scheidegger, A.E., and P. L. Willmore, 1957, The use of a least-squares
    method for the interpretation of data from seismic surveys, Geophys.,
    vol. 22, no. 1, p. 9.

Slemmons, D.B., A. E. Jones, and J. Gimlett, 1965, Catalog of Nevada
    earthquakes, 1852-1961, Bull. Seis. Soc. Am., vol. 55, p. 537.

Smith, J.J., J.S. Steinhart, and L. T. Aldrich, 1966, Lake Superior
    crustal structure, Jour. Geophys. Res., vol. 71, no. 4, p. 1141.

Steinhart, J.S., and T. J. Smith, 1966, Time-terms and structure in
    Western Lake Superior region, Am. Geophys. Union, Geophys. Mono-
    graph 10, p. 198.

Willmore, P.L., and A. M. Bancroft, 1960, The time-term approach to
    refraction seismology, Geophys. Jour., vol. 3, p. 419.

APPENDIX I

The following is a source listing of the computer program
developed for the time-term analysis. It was written in FORTRAN IV
for the University of Nevada computer Sigma 7. The program calculates
a least-squared refractor velocity from all available observations of
travel-times and distances; it calculates the residual (observed-
calculated travel-time) of each observation, determines the time-
term for each site, converts the time-terms into estimates of the
thickness of the upper layer by multiplying by $v_1/\sqrt{(1-v_1^2/v_2^2)}$, where
v_1 and v_2 are the velocities in the upper and lower layers, respectively.
Time-term solutions are also computed at various constrained velocities,
and the standard deviation of each solution determined from the formula

$$\sigma = \left[\frac{\sum_j \sum_i R_{ij}^2 \, \gamma_{ij}}{\sum_j \sum_i \gamma_{ij} - N} \right]^{1/2} \tag{Ia}$$

where

R_{ij} is the residual of an observation,

γ_{ij} is a statistical measure such that

$\gamma_{ij} = 1$, where R_{ij} exists and $= 0$, when it does not exist;

N is the number of sites (shot points + seismographic stations).

```
 1:        INTEGER SH,ST
 2:        READ(105,60) SH,ST
 3:        DIMENSION DIS(50,10),TT(50,10),P(50),R(10),F(10),C(50,10),D(50,10)
 4:       C,RES(50,10),G(50),A(50),B(50),TA(50),TB(10),DIJ(50,10),TIJ(50,10),
 5:       CRIJ(50,10)
 6:        COMMON DIS,TT,C,D,RES,DIJ,TIJ,RIJ
 7:        READ(105,10)((DIS(N,M),TT(N,M),M=1,ST),N=1,SH)
 8:        X=0
 9:        Y=0
10:        G=0
11:        E=0
12:        ALPHA=3.5
13:        V1=6.0
14:        DO15N=1,SH
15:        P(N)=0
16:        G(N)=0
17:        DO15M=1,ST
18:        P(N)=P(N)+TT(N,M)
19:        G(N)=G(N)+DIS(N,M)
20:     15 CONTINUE
21:        DO25M=1,ST
22:        F(M)=0
23:        R(M)=0
24:        DO25N=1,SH
25:        R(M)=R(M)+TT(N,M)
26:        F(M)=F(M)+DIS(N,M)
27:     25 CONTINUE
28:        DO35N=1,SH
29:        G=G+P(N)
30:     35 E=E+G(N)
31:        DO55N=1,SH
32:        DO55M=1,ST
33:        C(N,M)=-(1/ST)*P(N)+(1/(SH*ST))*G-(1/SH)*R(M)+TT(N,M)
34:        D(N,M)=-(1/ST)*G(N)+(1/(SH*ST))*E-(1/SH)*F(M)+DIS(N,M)
35:        X=X+(C(N,M)*D(N,M))
36:        Y=Y+(D(N,M)**2)
37:     55 CONTINUE
38:        WRITE(108,30)((C(N,M),M=1,ST),N=1,SH)
39:        WRITE(108,30)((D(N,M),M=1,ST),N=1,SH)
40:        V2=Y/X
41:        WRITE(108,20)V2
42:        DO65N=1,SH
43:        DO65M=1,ST
44:        RES(N,M)=C(N,M)-((1/V2)*D(N,M))
45:     65 CONTINUE
46:        WRITE(108,30)((RES(N,M),M=1,ST),N=1,SH)
47:        Z=0
48:        DO75M=1,ST
49:        B(M)=0
50:        DO75N=1,SH
51:        B(M)=B(M)+TT(N,M)=(DIS(N,M)/V2)
52:     75 CONTINUE
53:        DO85N=1,SH
54:        A(N)=0
55:        DO85M=1,ST
56:        A(N)=A(N)+TT(N,M)=(DIS(N,M)/V2)
57:     85 CONTINUE
58:        DO95N=1,SH
59:     95 Z=Z+A(N)
60:        DO115N=1,SH
```

```
61:          A(N)=((1/ST)*A(N))-(1/(SH*ST)*Z)+ALPHA
62:          TA(N)=A(N)*(V1/(SQRT(1-(V1**2)/(V2**2))))
63:    115 CONTINUE
64:          DO125M=1,ST
65:          B(M)=((1/SH)*B(M))-ALPHA
66:          TB(M)=B(M)*(V1/(SQRT(1-(V1**2)/(V2**2))))
67:    125 CONTINUE
68:          WRITE(108,40)(A(N),TA(N),N=1,SH)
69:          WRITE(108,70)(B(M),TB(M),M=1,ST)
70:          WRITE(108,50)((DIS(N,M),TT(N,M),M=1,ST),N=1,SH)
71:     10 FORMAT(12F6.1,/6F6.1)
72:     20 FORMAT(F5.3)
73:     30 FORMAT(9F8.3)
74:     40 FORMAT(2F15.3)
75:     70 FORMAT(2F20.3)
76:     50 FORMAT(18F6.1)
77:     60 FORMAT(2I10)
78:          DO145N=1,SH
79:          DO145M=1,ST
80:          TIJ(N,M)=DIS(N,M)/V2+A(N)+B(M)
81:          RIJ(N,M)=TT(N,M)-TIJ(N,M)
82:    145 CONTINUE
83:          WRITE(108,30)((RIJ(N,M),M=1,ST),N=1,SH)
84:          DO45V3=7.7,7.8,0.01
85:          SUM=0
86:          Z=0
87:          DO185N=1,SH
88:          A(N)=0
89:          DO185M=1,ST
90:          A(N)=A(N)+TT(N,M)-(DIS(N,M)/V3)
91:    185 CONTINUE
92:          DO195N=1,SH
93:    195 Z=Z+A(N)
94:          DO155N=1,SH
95:          A(N)=((1/ST)*A(N))-(1/(SH*ST)*Z)+ALPHA
96:          TA(N)=A(N)*(V1/(SQRT(1-(V1**2)/(V3**2))))
97:    155 CONTINUE
98:          DO165M=1,ST
99:          B(M)=0
100:          DO165N=1,SH
101:          B(M)=B(M)+TT(N,M)-(DIS(N,M)/V3)
102:    165 CONTINUE
103:          DO175M=1,ST
104:          B(M)=((1/SH)*B(M))-ALPHA
105:          TB(M)=B(M)*(V1/(SQRT(1-(V1**2)/(V3**2))))
106:    175 CONTINUE
107:          DO135N=1,SH
108:          DO135M=1,ST
109:          TIJ(N,M)=DIS(N,M)/V3+A(N)+B(M)
110:          DIJ(N,M)=TT(N,M)-TIJ(N,M)
111:          SUM=SUM+(DIJ(N,M)**2)
112:    135 CONTINUE
113:          STD=SQRT(SUM/103)
114:          WRITE(108,80)V3,STD
115:          WRITE(108,40)(A(N),TA(N),N=1,SH)
116:          WRITE(108,70)(B(M),TB(M),M=1,ST)
117:          WRITE(108,30)((DIJ(N,M),M=1,ST),N=1,SH)
118:     45 CONTINUE
119:     80 FORMAT(2F15.3)
120:          STOP
121:          END
```